Global Biogeochemical Cycles

RESEARCH ARTICLE
10.1029/2022GB007389

Special Section:
Southern Ocean and Climate: Biogeochemical and Physical Fluxes and Processes

Vertical Structure in Phytoplankton Growth and Productivity Inferred From Biogeochemical-Argo Floats and the Carbon-Based Productivity Model

Lionel A. Arteaga[1,2,3], Michael J. Behrenfeld[4], Emmanuel Boss[5], and Toby K. Westberry[4]

[1]Global Modeling and Assimilation Office, NASA Goddard Space Flight Center, Greenbelt, MD, USA, [2]Goddard Earth Sciences, Technology and Research II, University of Maryland Baltimore County, Baltimore, MD, USA, [3]Program in Atmospheric and Oceanic Sciences, Princeton University, Princeton, NJ, USA, [4]Department of Botany and Plant Pathology, Oregon State University, Corvallis, OR, USA, [5]School of Marine Sciences, University of Maine, Orono, ME, USA

Abstract Estimates of marine net primary production (NPP) commonly rely on limited in situ ^{14}C incubations or satellite-based algorithms mainly constrained to the surface ocean. Here we combine data from biogeochemical Argo floats with a carbon-based productivity model (CbPM) to compute vertically resolved estimates of NPP. Inferred NPP profiles derived by informing the CbPM with float-based, depth-resolved, bio-optical data are able to qualitatively reproduce the vertical structure in NPP inferred from in situ ^{14}C incubations at various ocean regions. At station ALOHA, float-based estimates agree within uncertainty with productivity observations at depth, but underestimate surface NPP. We test the ability of the CbPM to infer the depth-resolved structure in NPP from bio-optical properties in the mixed layer, in similar fashion as how remote sensing algorithms of ocean productivity operate. In Southern Ocean waters, the depth-reconstructing implementation of the CbPM overestimates phytoplankton division rates and Chl:C below the mixed layer, resulting in artificially high subsurface NPP when compared with the fully float-informed implementation of the model. The CbPM subsurface extrapolation of phytoplankton Chl, Chl:C, division rates, and NPP improves by accounting for deep nutrient (iron) stress impacts on photoacclimation in the Southern Ocean. This improvement is also observed in vertically integrated NPP, where the mean bias between model implementations in depth-integrated productivity south of 30°S is reduced by 62% when account for deep iron limitation. Our results demonstrate that profiling data from biogeochemical Argo floats can serve to inform regional adjustments that lead to the improvement of marine productivity algorithms.

Plain Language Summary The oceanic production of organic carbon by photosynthesis is a key process that regulates marine food-webs and the planet's climate. This production takes place not only at the surface of the ocean, but also in the subsurface, where it is difficult for ocean-viewing satellites to retrieve accurate information. In this work, we combine information on water column biogeochemical properties collected by bio-optical sensors on autonomous profiling floats with a mathematical model to estimate biological primary production throughout the water column. Our results show that this combination of model and float data can reproduce depth profiles of productivity observed in various ocean regions. We also test the ability of the model to infer subsurface productivity in Southern Ocean waters based on information of averaged biogeochemical properties in the surface ocean mixed layer alone. We find that the model improves the estimation of subsurface productivity when accounting for the limiting effect of scarce nutrients in Antarctic waters, such as iron. Our results provide confidence in the combination of float data and existing models to describe the vertical structure in marine biological productivity, and guide the improvement of productivity algorithms in specific regions of the global ocean.

Key Points:

- Net primary production (NPP) estimates from the float-informed carbon-based productivity model (CbPM) can reproduce the vertical structure in ^{14}C-based productivity observed in various ocean regions
- Accounting for deep iron limitation improves the reconstruction of depth-resolved biomass and productivity by the CbPM in the Southern Ocean
- The inclusion of deep iron limitation potentially reduces the bias in Southern Ocean estimates of depth-integrated NPP by 62%

Supporting Information:

Supporting Information may be found in the online version of this article.

Correspondence to:

L. A. Arteaga,
lionel.arteagaquintero@nasa.gov

Citation:

Arteaga, L. A., Behrenfeld, M. J., Boss, E., & Westberry, T. K. (2022). Vertical structure in phytoplankton growth and productivity inferred from Biogeochemical-Argo floats and the carbon-based productivity model. *Global Biogeochemical Cycles*, *36*, e2022GB007389. https://doi.org/10.1029/2022GB007389

Received 14 MAR 2022
Accepted 15 AUG 2022

Author Contributions:

Conceptualization: Lionel A. Arteaga
Data curation: Lionel A. Arteaga
Formal analysis: Lionel A. Arteaga, Michael J. Behrenfeld, Emmanuel Boss, Toby K. Westberry
Funding acquisition: Lionel A. Arteaga
Investigation: Lionel A. Arteaga, Michael J. Behrenfeld, Emmanuel Boss, Toby K. Westberry

1. Introduction

Marine net primary production (NPP) is an essential biogeochemical process that represents the gateway of carbon into the marine ecosystem via the production of organic matter from dissolved inorganic carbon (DIC), nutrients, and light. Understanding and quantifying marine NPP is of major importance since it accounts for about half of the global production in the biosphere (Field, 1998) and it is the primary source of chemical energy sustaining marine trophic webs. In situ measurements of NPP are commonly obtained employing the ^{14}C method, where the rate of carbon fixation by autotrophs is measured by tracing the uptake of radioactive ^{14}C from

Methodology: Lionel A. Arteaga, Michael J. Behrenfeld, Emmanuel Boss, Toby K. Westberry
Resources: Lionel A. Arteaga
Software: Lionel A. Arteaga
Validation: Lionel A. Arteaga, Michael J. Behrenfeld
Visualization: Lionel A. Arteaga
Writing – original draft: Lionel A. Arteaga
Writing – review & editing: Lionel A. Arteaga, Michael J. Behrenfeld, Emmanuel Boss

dissolved inorganic into particulate organic form (Cullen, 2001; Steemann Nielsen, 1952). While the ^{14}C method has become the standard in the oceanographic community for measuring carbon assimilation (i.e., productivity) rates, its application in the marine environment is labor intensive, limiting its routine implementation in the field and resulting in scarce temporally and spatially resolved observations of marine productivity throughout the global ocean.

Satellite-based ocean color models are the most frequently used tool to obtain global and regional estimates of marine productivity (McClain, 2009). Ocean color observations rely on the detection of spectral variations in water-leaving radiance to infer the concentration of dominant biotic constituents in the water (Groom et al., 2019). NPP models based on ocean color leverage the high temporal and spatial resolution of satellite observations (pixel size ~1–10 km), capable of providing repeated global coverage every 2–3 days at the equator and daily coverage at higher latitudes (IOCCG, 2008). Despite the obvious benefits and advantages of employing remote sensing to study upper ocean ecosystems and productivity, an important caveat of these observations is that they are mostly limited to the mixed surface ocean (specifically, the first optical depth) and unable to resolve subsurface dynamics, with the potential exception of ocean-based light detection and ranging (lidar) technologies (Hostetler et al., 2018).

An emerging array of sensors capable of sampling the vertical water column with adjustable frequency is being deployed on board of a network of drifting Biogeochemical-Argo (BGC-Argo) floats (Chai et al., 2020; Claustre et al., 2020). Sensors on BGC-Argo floats vary, but they can enable the observation of as many as six essential biogeochemical and bio-optical variables: oxygen, nitrate, pH, fluorescence-based chlorophyll *a*, suspended particles from optical backscattering, and downwelling irradiance, in addition to the standard conductivity-temperature-depth (CTD) sensors. These data permit the estimation and analysis of vertically resolved NPP rates, providing a three-dimensional view of primary productivity in the ocean. More specifically, vertical profiles of fluorescence-based chlorophyll *a* (Chl) and phytoplankton carbon biomass derived from particle backscattering (b_{bp}) can be used to model vertically resolved phytoplankton division rates (μ) based on the physiological state of the cells, inferred from variations in the cellular chlorophyll to carbon ratio (Chl:C) (Behrenfeld et al., 2005). This approach of parametrizing phytoplankton growth and productivity based on Chl:C variability is encapsulated by the Carbon-based Productivity Model (Westberry et al., 2008, CbPM), which is an ocean NPP model developed to include information on the subsurface light field and nitracline depths to parameterize photoacclimation and nutrient stress throughout the water column. The CbPM lends itself well for BGC-Argo floats applications since (a) it was originally designed to describe the subsurface structure in ocean productivity, and (b) division rates are parametrized from variations in phytoplankton Chl:C, a property that can be inferred from standard bio-optical sensors on BGC-Argo floats. The now widespread availability of BGC-Argo data provides an opportunity to assess the CbPM's ability of modeling surface (Long et al., 2021) and subsurface phytoplankton physiology and productivity (Arteaga et al., 2020; Estapa et al., 2019; Yang et al., 2021).

In this work, we use vertically resolved BGC-Argo data to inform the CbPM and compute phytoplankton growth and productivity. The float data set, composed of paired biogeochemical and bio-optical profiles, was obtained from the Southern Ocean Carbon and Climate Observations and Modeling (SOCCOM) program (Johnson et al., 2017; Riser et al., 2018). This data set consists mostly of Southern Ocean data (south of 30°S), although float data from subtropical and high latitudes regions in the northern hemisphere are also available and analyzed (Figure S1 in Supporting Information S1).

The next sections of this paper are structured as follows: Sections 2.1 and 2.2 describe the general characteristic of the BGC-Argo float data and computation of phytoplankton biomass (chlorophyll and carbon) from bio-optical measurements. Section 2.3 describes the principal components of the CbPM growth equations (Section 2.3.1), the parameterization of photoacclimation at depth (Section 2.3.2), and details the different implementations of the model in this study (Section 2.3.3). These implementations can be divided in two main categories, (a) application of CbPM's growth equations to vertically resolved float data, and (b) inference of the subsurface vertical profile in phytoplankton biomass, growth parameters, and productivity from float measurements in the surface mixed layer, in similar fashion as how the satellite-based CbPM operates. Section 2.4 describes the use and application of satellite irradiance data to obtain float-based NPP estimates. Section 2.5 describes two in situ observational data sets: the first one (Section 2.5.1) is a published data set of compiled vertically resolved in situ ^{14}C-based productivity measurements (Marra et al., 2021) employed to assess the ability of the model in reproducing the general vertical structure of NPP at different ocean regions. The second data set (Section 2.5.2) includes in situ ^{14}C-based

productivity, fluorometric chlorophyll *a*, and phytoplankton carbon measurements at station ALOHA. Here we also describe satellite ocean color data used for a comparison exercise at this station. In Section 3.1 we compare regional ^{14}C-based observations with productivity estimates obtained from the application of the CbPM to vertically resolved float-based chlorophyll and carbon biomass throughout the water column. Section 3.2 compares the impact that different implementations of the CbPM have on the computation of vertically resolved NPP in the Southern Ocean, and how model outputs from this region compare with those observed in station ALOHA. This section also discusses an emerging latitudinal relationship between the vertical gradient in nitrate observed in binned float profiles and estimates of the base of the productive layer, euphotic depth, and isolume, obtained from combining the CbPM and float data. Section 3.3 evaluates the impact that different implementations of the CbPM have on the computation of vertically integrated NPP. We provide our final conclusions in Section 4.

2. Methods

2.1. BGC-Argo Data

Quality-controlled float data analyzed in this study were downloaded from the Southern Ocean Carbon and Climate Observations and Modeling (SOCCOM) data portal (https://soccom.princeton.edu/content/data-access). Specifically, we obtained the 20 April 2020 low-resolution data snapshot (with LIAR-based estimation of carbon chemistry variables, not used) published in a NetCDF format (Johnson et al., 2020). This float data set contains a total of 28,462 vertical profiles of paired biogeochemical measurements taken between 2007 and 2020, with most of the profiles being taken after 2012. In this work we focus our analyses on profiles obtained between 01 January 2012 and 20 April 2020. Most BGC-Argo floats in this data set were equipped with CTD, oxygen, nitrate, pH and bio-optical sensors (fluorescence and particulate backscattering at 700 nm (b_{bp} (700)) (Johnson et al., 2017). Our analysis focuses on floats with bio-optical sensors, which are essential to compute NPP. SOCCOM-deployed BGC-Argo floats sample the vertical water column every 5 or 10 days, depending on the preset programming of the float, with most floats sampling every 10 days. The vertical resolution of the measurements taken by the floats varies with depth, with measurements every 5 m in the upper 100 m. The uppermost sampled depth is ~5 or 7 m below surface. Float observations at this depth are extrapolated to the surface. Vertical sampling resolution decreases to 10 m below 100 m depth, 20 m below 360 m depth, and 50 m between 400 and 2000 m depth. Vertical profiles of float data are interpolated to a 1 m resolution and smoothed using a seven point running-median filter (Arteaga et al., 2020; Boss & Behrenfeld, 2010). Most profiles correspond to the Southern Ocean region south of 30°S, but profile information from other regions such as the western and central North Pacific, the Sub-Arctic North Atlantic, and the Arabian Sea are also included (Figure S1 in Supporting Information S1). Nitrate data analyzed in this work are also obtained from paired float measurements. The mixed layer depth (MLD) is estimated using float in situ temperature and salinity profiles following de Boyer Montégut et al. (2004). All data were analyzed in Python 3.9.7.

2.2. Estimates of Phytoplankton Carbon and Chlorophyll

Phytoplankton carbon (C_{phyto}) and chlorophyll estimates are obtained from bio-optical measurements (profiles) of b_{bp} (700) and fluorescence made by the BGC-floats. For each b_{bp} (700) profile we subtract the mean estimated concentration between 900 and 1,000 m from the entire vertical profile, in order to make sure that phytoplankton carbon asymptotes toward zero at depth (similarly as in Arteaga et al., 2020). The particle backscatter at 470 nm (b_{bp} (470)) is estimated from b_{bp} (700) following a power law function with an exponent of −1 (Morel & Maritorena, 2001):

$$b_{bp}(470) = b_{bp}(700)\left(\frac{470}{700}\right)^{-1} \quad (1)$$

C_{phyto} is inferred from an empirical relationship with b_{bp} (470) (Graff et al., 2015):

$$C_{phyto} = 12128 \times b_{bp}(470) + 0.59 \quad (2)$$

This empirical relationship between C_{phyto} and b_{bp} (470) is based on a global data set of backscattering and flow cytometric determinations of phytoplankton and has been employed in similar computations of float-based primary productivity in the North Atlantic (Estapa et al., 2019; Yang et al., 2021).

Chlorophyll concentration (mg m^{-3}) is obtained from float fluorescence measurements, adjusted by a calibration factor of $\frac{1}{2}$ applied to profiles north of 30°S (Roesler et al., 2017). Float profiles south of 30°S were adjusted by a factor of $\frac{1}{6}$ based on surface (depth <100 m) High Performance Liquid Chromatography (HPLC) measurements from chlorophyll samples taken during early SOCCOM float deployments in the Southern Ocean (see Johnson et al., 2017; Boss & Haëntjens, 2016, for details). This adjustment factor of $\frac{1}{6}$ to float fluorescence-based data in the Southern Ocean yields estimates of Chl that agree well with satellite ocean color retrievals in this region (Haëntjens et al., 2017). Lastly, profiles with sun elevation >0 were corrected for non-photochemical quenching (NPQ) following Xing et al. (2012).

2.3. Carbon-Based Productivity Model (CbPM)

2.3.1. CbPM Growth Equations

The CbPM estimates phytoplankton division rate as a function of the Chl:C ratio at each depth (z). The Chl:C ratio serves as an indicator of phytoplankton nutrient and light stress, where nutrient stress is assessed by removing the light effect on Chl:C based on observed submarine light levels and a photoacclimation model. Specifically, the cellular nutrient index (I_{nut}) is inferred from the relative difference between the actual local Chl:C ratio, the Chl:C value when $\mu = 0$ ($Chl:C_{\mu=0} = 3 \times 10^{-4}$, Westberry et al., 2008), and the theoretical maximum Chl:C achieved under replete nutrient conditions at the local light level ($Chl:C_{max}$) (Behrenfeld et al., 2005; Westberry et al., 2008):

$$I_{nut}(z) = \frac{Chl:C(z) - Chl:C_{\mu=0}}{Chl:C_{max}(z) - Chl:C_{\mu=0}} \quad (3)$$

$$Chl:C_{max}(z) = 0.022 + (0.045 - 0.022) \times \exp^{(-3.0\ PAR(z)daylength)} \quad (4)$$

The cellular light index (or light limitation term), I_{light}, is a function of the local light level at each depth:

$$I_{light}(z) = 1 - \exp^{(-5\ PAR(z))} \quad (5)$$

Finally, phytoplankton division rate (μ) at each depth is a function of the maximum potential division rate ($\mu_{max} \approx 2$, Banse, 1991), I_{nut}, and I_{light}:

$$\mu(z) = \mu_{max} \times I_{nut}(z) \times I_{light}(z) \quad (6)$$

NPP is the product of local μ and C_{phyto}

$$NPP(z) = \mu \times C_{phyto} \quad (7)$$

Equations 3–7 can be directly combined with (satellite or float) irradiance data and phytoplankton biomass estimates (Chl and C_{phyto}) derived from float bio-optical data to compute phytoplankton division rates and NPP.

2.3.2. Photoacclimation and Nutrient Stress in the Original CbPM

Photoacclimation in phytoplankton is defined as a physiological response of cells to increase or maintain division rates under declining light levels, evidenced by an increase in cellular Chl:C ratio. Here, we review briefly the mathematical description of photoacclimation at depth presented in the original depth-resolving CbPM (Westberry et al., 2008). In the CbPM developed for satellite applications, the model infers the local Chl:C ratio at each depth (z) in order to reconstruct the vertical profile of phytoplankton productivity below the surface mixed layer depth. The photoacclimation response is modeled as a function of the ambient light and can also be affected by a potential relaxation of nutrient stress according to distance from the nitracline:

$$Chl:C_{max}(z) = 0.022 + (0.045 - 0.022) \times \exp^{(-3.0\ PAR(z)daylength)} - \Delta Chl:C_{Nut}\left(1 - e^{-0.075\Delta zNO3}\right) \quad (8)$$

The first term in Equation 8 is identical to Equation 4, while the second term accounts for potential nutrient relaxation with depth below the mixed layer. $\Delta Chl:C_{Nut}$ infers nutrient stress in the mixed layer as the difference between satellite-derived mean Chl:C ratio and the maximum potential Chl:C ratio for a given irradiance

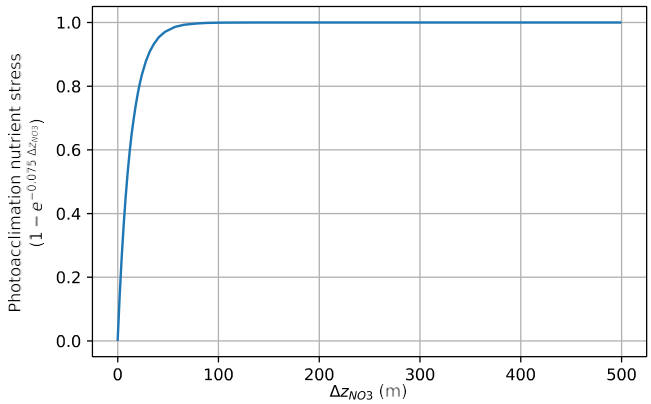

Figure 1. Relationship between the distance separating any given depth below mixed layer depth and the nitracline (Δz_{NO3}) versus the modeled photoacclimation nutrient stress below the mixed layer ($1-e^{-0.075\Delta z_{NO3}}$) in the original carbon-based productivity model (Westberry et al., 2008).

within the mixed layer. Δz_{NO3} is the distance from the nitracline, valid for depths shallower than the nitracline and below the MLD. A very deep nitracline ($\Delta z_{NO3} \rightarrow \infty$) maximizes nutrient stress to the degree inferred within mixed layer (i.e., second term in Equation 8 approaches $\Delta Chl{:}C_{Nut}$). As the nitracline shallows and approximates a given depth below the MLD ($\Delta z_{NO3} \rightarrow 0$), nutrient stress diminishes (i.e., second term in Equation 8 approaches zero) (Figure 1). The exponent in Equation 8 of 0.075 gives an e-folding of 13 m and approximates a "smooth" boundary due to diffusion and diapycnal mixing across the nitracline (Westberry et al., 2008).

2.3.3. CbPM Implementations

The original CbPM, developed for satellite-based applications, infers depth-resolved phytoplankton biomass, division rates (μ), and NPP profiles from satellite-based surface information of incident light, phytoplankton carbon, and chlorophyll. As indicated above, by "original" we refer to the version described in Westberry et al. (2008), which builds upon a yet previous version of this model (Behrenfeld et al., 2005) to provide vertically resolved (not just vertically integrated) estimates of NPP. The satellite-informed version of the CbPM ($CbPM_{Sat}$) is not the focus of this study, but it is briefly used to assess discrepancies between float-based and in situ productivity profiles at station ALOHA (see details in Section 2.5.2).

In this work we implement the CbPM in three distinct configurations (Table 1): The first implementation directly uses float-derived profiles of phytoplankton biomass and Chl:C ratio to estimate NPP following the growth equations of the model (Equations 3–7 in Section 2.3.1), hereafter referred to as $CbPM_{Argo}$. In order to gain an insight into how well can the fully float-informed productivity model reproduce NPP profiles throughout the water column, we compare depth-resolved productivity profiles (within and below the mixed layer) obtained from the $CbPM_{Argo}$ against available depth-resolved in situ ^{14}C-based NPP observations scattered throughout various ocean regions (Section 2.5.1). The comparison with in situ data serves as a base step to assess the following implementations of the model.

The second implementation operates in similar fashion as the satellite-based model, inferring vertical profiles of phytoplankton biomas, Chl:C ratio, and productivity from averaged float information in the upper ocean mixed layer, hereafter referred to as $CbPM_{Orig}$. The SOCCOM float data set is biased toward latitudes south of 30°S, where iron, and not nitrate, is considered the primary limiting nutrient of marine productivity (Boyd et al., 2007; Martin et al., 1990). Thus, the standard configuration of $CbPM_{Orig}$, which uses nitracline depths to parameterize photoacclimation and nutrient stress throughout the water column, is likely to fail in this region and others where nitrate is not the primary limiting nutrient. The nitracline depth is here defined based on paired float nitrate profiles as the depth where nitrate exceeds 0.5 μ mol kg^{-1} (similarly as for the satellite-based version of the model described in Westberry et al., 2008). In an effort to broaden the applicability of the model, we include a modification where for waters south 30°S the nitracline is substituted by a constant ferricline depth, and for waters north of 30°S where the depth of nitrate >0.5 μ mol kg^{-1} is shallower than the depth of the mixed layer,

Table 1
Implementation of the Carbon-Based Productivity Model Used in This Study

	$CbPM_{Argo}$	$CbPM_{Orig}$	$CbPM_{Mod}$
Above MLD	Depth-resolved or averaged, based on float obs.	Averaged based on float obs.	Averaged based on float obs.
Below MLD	Depth resolved based on float obs.	Depth resolved reconstructed (as in satellite applications)	Depth resolved reconstructed (as in satellite applications)
Nutrient stress north of 30°S	Based on local Chl:C (z)	Nitracline depth (>0.5 μ mol kg^{-1})	Nitracline depth (>0.5 μ mol kg^{-1}) or depth of maximum nitrate gradient when nitracline depth < MLD.
Nutrient stress south of 30°S.	Based on local Chl:C (z).	Nitracline depth (>0.5 μ mol kg^{-1})	Ferricline depth (333 m)

the nitracline is defined by the depth of strongest gradient in nitrate concentration. Given that current BGC-Argo floats do not have iron-detecting sensors, the constant ferricline was defined at 333 m, which was the mean ferricline depth found across 140 unique determinations within the Southern Ocean (Tagliabue et al., 2014). This modified version of the model is hereafter referred to as $CbPM_{Mod}$ (Table 1). It is important to note that the "satellite-oriented" implementations of the model ($CbPM_{Orig}$ and $CbPM_{Mod}$) use the "nutricline" to simulate the regulation of the Chl:C ratio as a result of photoacclimation below the mixed layer, which impacts μ via Equations 3 and 8. This information is not pertinent to the $CbPM_{Argo}$, where the Chl:C ratio is not modeled but set by the bio-optical float profiles. The $CbPM_{Orig}$ and $CbPM_{Mod}$ follow the code developed for satellite applications substituting remotely sensed inputs by mean mixed layer Chl and C_{phyto} from the floats. The complete code for the satellite-based CbPM is available at http://sites.science.oregonstate.edu/ocean.productivity/cbpm2.code.php. The adapted code used in the $CbPM_{Argo}$ to compute depth-resolved NPP based on float-derived Chl and C_{phyto} profiles is available at https://zenodo.org/record/6599224#23.YqJZFC1h3uM (Arteaga, 2022).

We assess differences between the three different implementations of the model ($CbPM_{Argo}$, $CbPM_{Orig}$, and $CbPM_{Mod}$) by comparing meridional trends in depth-resolved zonal-averages of phytoplankton biomass, growth parameters, and NPP. For this comparison, we compute the $CbPM_{Argo}$ by averaging phytoplankton biomass properties (Chl and C_{phyto}) within the mixed layer, in the same manner as for the $CbPM_{Orig}$, and $CbPM_{Mod}$. This permits a fair and correct comparison of productivity and biomass inferred by the $CbPM_{Orig}$, and $CbPM_{Mod}$, since these implementations are unable to resolve dynamics in phytoplankton productivity within the mixed layer (similarly as for the satellite-based CbPM). In this comparison, data are first binned into a 1° by 1° grid and averaged zonally and temporally, providing a climatological view of productivity within the time that floats have been deployed (float profile abundance increased mostly over the last 5 years). The comparison between model implementations is restricted to the Southern Ocean, since this region has sufficient float profiles to effectively compute robust meridional sections based on zonally averaged data. We then extend the meridional sections to include data from the northern hemisphere and discuss an emerging latitudinal relationship between the vertical gradient in nitrate observed in binned float profiles and estimates of the base of the productive layer, euphotic depth, and isolume, obtained from the $CbPM_{Argo}$ (with float inputs averaged in the mixed layer). However, it is important to note that binned data in the northern hemisphere are mostly representative of defined geographical regions such as the North Pacific Central Gyre, Sub-Arctic North Atlantic, and the Arabian Sea (Figure S1 in Supporting Information S1).

Differences in depth-integrated NPP between the three implementations of the CbPM are assessed based on ungridded vertical profiles. Each CbPM implementation was computed by averaging phytoplankton biomass properties within the mixed layer (as above). NPP is integrated over the upper 200 m, the depth at which local depth-resolved NPP has already reached negligible values in all profiles.

2.4. Satellite Irradiance Data for Float-Based NPP

The underwater light field of all CbPM implementations is depth- and spectrally resolved based on surface ocean photosynthetically available radiation (PAR), float Chl information, and constant spectral fractions from an atmospheric radiative transfer model (Ricchiazzi et al., 1998). Given that floats analyzed in this study were not equipped with light sensors, the Argo-CbPM works similarly as the satellite-based CbPM inferring the underwater light field from estimates of surface PAR (E m^{-2} d^{-1}) obtained from satellite data downloaded from the NASA Ocean Color website (https://oceancolor.gsfc.nasa.gov). Daily global maps of MODIS-Aqua PAR (L3, 4km) are obtained for the period between 01 January 2012 and 20 April 2020. Satellite matchups to float profiles are obtained for the same day and the closest pixel to the spatial position of each float profile. Profiles with unknown location (including under ice profiles) are assigned NaN as PAR data matchup. The satellite PAR product is not computed (NaN assigned) if Top-of-Atmosphere radiance is negative or solar zenith angle exceeds 90°.

2.5. In Situ Observations

2.5.1. Global ^{14}C-Based NPP Data

We compare our modeled float productivity estimates derived from the $CbPM_{Argo}$ (within and below the mixed layer) with ^{14}C-based NPP observations compiled by Marra et al. (2021). This compilation was deliberately curated to only include incubations done in situ (not on deck incubators). On deck incubations may experience

photo-inhibiting levels of irradiance and lower carbon assimilation near the surface compared to in situ incubations, which tend to be exposed to a higher sun angle (lower zenith angle) during sunrise and sunset, resulting in greater reflection and less irradiance entering the surface layers (Barber et al., 1997, 2001; Marra et al., 2021). We searched for available float profiles in all stations where cruises took samples that were included in the observational data base (cruises can be sorted out by "Cruise_Designation" in the data base: http://dmoserv3.bco-dmo.org/jg/serv/BCO-DMO/ISPP14C/c14_primary_prod.html0%7Bdir=dmoserv3.whoi.edu/jg/dir/BCO-DMO/ON_DEQUE3/,info=dmoserv3.bco-dmo.org/jg/info/BCO-DMO/ISPP14C/c14_primary_prod%7D). In order to maximize the amount of float and in situ comparisons of productivity profiles, we defined a variable perimeter around each field observational station (geographical boundaries are listed in Table S1 in Supporting Information S1). Subsampled float profiles at each observational station were obtained at the same months as observations. However, given the disparity between data sets, the total number of float profiles in a given month/station is not necessarily the same as for in situ observations. In situ data included in the final comparison were obtained between 1985 and 1998, while the earliest float profile in the final data set analyzed is from 2012. Discrepancies in the collection of float and in situ productivity data imply that no "true matchups" are available to quantitatively evaluate the skill of the CbPM. Our aspiration is that despite the multiple disparities between the float and observational data sets, we are able to qualitatively compare distinctive features of the vertical structure in NPP imposed by the seasonality and unique biogeochemical properties of each region. Regions with available NPP profiles for comparison between float estimates and the Marra et al. (2021) data set are (number of cruises/stations): The Ross Sea (1), Southern Polar Front (2), North Pacific Central Gyre (1), Sub-Arctic North Atlantic (2), and the Arabian Sea (6) (See Table S1 in Supporting Information S1 for specific details of each cruise/station and float profiles comparisons).

2.5.2. ALOHA Data

CbPM outputs are also compared against in situ data from station ALOHA (part of the Hawaii Ocean Time-series (HOT) program), located at 22° 45'N, 158°W. This station has a large historical record of depth-resolved ^{14}C-based productivity and fluorometric chlorophyll measurements available since 1989 (Karl et al., 2021). Also available for the period 2004–2014 are estimates of phytoplankton carbon obtained from a combination of epi-fluorescence and flow-cytometry methods. Data were obtained via the Hawaii Ocean Time-series HOT-DOGS application (http://hahana.soest.hawaii.edu/hot/hot-dogs/). Depth-resolved NPP, Chl, and C_{phyto} data were averaged in depth bands of ±1 m around the following depths: 5 m, 25 m, 45 m, 75 m, 100 m, 125 m, 150 m, 175 m, and sorted into seasonal climatologies. For this comparison exercise at station ALOHA we also obtained output from the original CbPM (Westberry et al., 2008) forced with climatological satellite ocean color data ($CbPM_{Sat}$). These data include MODIS-Aqua (L3, 9km) monthly climatologies for the period 2003 and 2017 of surface chlorophyll, particulate backscattering at 443 nm ($b_{bp}(443)$)), and PAR downloaded from the NASA Ocean Color website (https://oceancolor.gsfc.nasa.gov). The overall model implementation, including the estimation of phytoplankton carbon from b_{bp} (443), followed the methods described in Westberry et al. (2008). The model was informed with satellite data for a 1° box surrounding the nominal ALOHA site. MLD inputs were obtained from monthly climatologies for the same period (2003–2017) from the HYbrid Coordinate Ocean Model (HYCOM) (Bleck, 2002) (available at http://orca.science.oregonstate.edu/2160.by.4320.monthly.hdf.mld030.hycom.php). The nitracline (0.5 μ mol kg^{-1} NO_3^- threshold) was calculated from a globally interpolated, monthly resolved, nitrate climatology from the World Ocean Atlas 2013 V2 (Garcia et al., 2014).

3. Results and Discussion

3.1. Comparison of the $CbPM_{Argo}$ and Depth-Resolved ^{14}C-Based Observations

We compare fully vertically resolved (within and below the mixed layer) NPP profiles from the $CbPM_{Argo}$ against depth-resolved in situ ^{14}C-based observations of productivity (Marra et al., 2021) (Figure 2 and S2 in Supporting Information S1). Available float-based productivity profiles in each station are averaged (black lines), while individual ^{14}C incubations within each cruise profile are first linearly interpolated with depth and subsequently averaged (red lines). Averaged depth-resolved profiles from the $CbPM_{Argo}$ generally capture the distinct vertical structure and broad-scale magnitude of averaged in situ primary productivity profiles in contrasting bio-geographical regions: Southern Ocean, North Pacific Gyre, Sub-Arctic North Atlantic (Figure 2), and Arabian Sea (Figure S2 in Supporting Information S1). In the Southern Ocean, observational cruise data are available in the Ross Sea (one station) and around the Polar Front (two stations). In the Ross sea (Figure 2a),

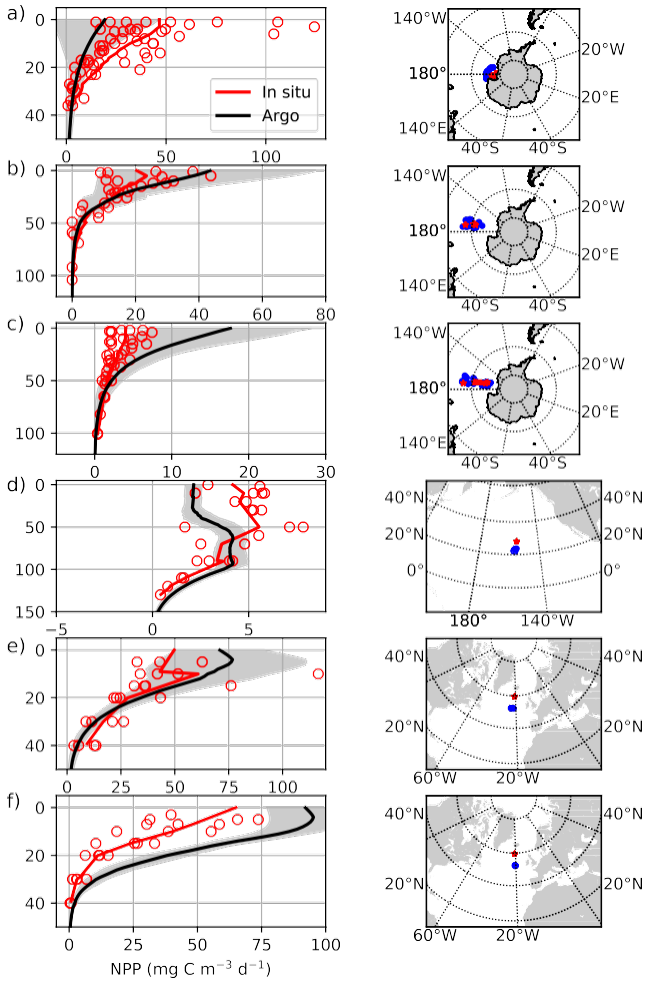

Figure 2. (left panels) In situ ^{14}C-based net primary production (NPP) measurements (open red circles) and averaged float-based NPP profiles obtained from the carbon-based productivity model$_{Argo}$ (black line ± standard deviation represented by the gray-shaded area). Red line represents the average of depth-interpolated in situ profiles. (right panels) Geographical location of in situ ^{14}C-based productivity profiles (red filled circles) and float NPP profiles (blue filled circles) for various ocean regions (Cruise_Designation): (a) Ross Sea (NBP-97-1), (b) Polar Front (rr-kiwi-7), (c) Polar Front (rr-kiwi-9), (d) North Pacific Gyre (Alcyone-III), (e) Sub-Arctic North Atlantic (EN 224), (f) Sub-Arctic North Atlantic (EN 227) (See Table S1 in Supporting Information S1 for specific details of each cruise/station).

mean float-based surface productivity is lower than in observations, while for station rr-wiki-7 in the Polar Front (Figure 2b), float-based NPP is closer in magnitude to ^{14}C-incubations and both (float-based and observational profiles) follow a similar attenuation of productivity with depth. Station rr-wiki-9, also in the Polar Front (Figure 2c), shows a similar vertical structure in float and ^{14}C-based averaged profiles as for station rr-wiki-7, but the averaged float productivity profile is higher than the average observational profile. All Southern Ocean stations follow a monotonic decrease in productivity with depth, except for a slight increase observed in ^{14}C-incubations within the upper 20 m at station rr-wiki-7 (Figure 2b). The magnitude and shape of the mean vertical NPP profile of the Southern Ocean stations (Figures 2a–2c) contrast those of the North Pacific Gyre (Figure 2d), where float-based and ^{14}C-based productivity are on average between 0 and 5 mg C m^{-3} d^{-1} in the upper 100 m (compared with a range from 0 to 50 mg C m^{-3} d^{-1} for averaged productivity profiles in Southern Ocean stations). In the North Pacific Gyre, both averaged float-based and ^{14}C-based profiles show a subsurface productivity maximum at about 50 m. Here, the averaged float NPP profile increases with depth within the upper 50 m, while ^{14}C-based observations present a less pronounce increase in NPP given that surface ^{14}C-incubations yielded higher surface productivity estimates to begin with. In the Sub-Arctic North Atlantic (Figures 2e and 2f), the range in averaged surface float- and ^{14}C-based productivity profiles is between 0 and nearly 100 mg C m^{-3} d^{-1}, closer in magnitude to the surface productivity range of the high latitude Southern Ocean stations. Mean vertical profiles (float- and ^{14}C-based) in the Sub-Arctic North Atlantic show a rapid attenuation of productivity with depth, analogous to the Southern Ocean stations and in constrast to what is observed in the mid latitude North Pacific Gyre. Six additional stations with available float- and ^{14}C-based productivity profiles are present for cruises conducted in the Arabian Sea (Figure S2 in Supporting Information S1). Overall, there is good qualitative agreement in the vertical structure of the productivity profile between floats and observations for all stations/cruises compared in this region.

All the individual in situ and float-based productivity profiles included in each of the stations above correspond to the spring-summer season in each hemisphere (Table S1 in Supporting Information S1). Nevertheless, there are many disparities in the collection of float-based and ^{14}C-based observational profiles that prevent a formal quantitative validation of the productivity output derived from the CbPM$_{Argo}$. In situ and float profiles are not exact paired estimates in space and time, with ^{14}C-based productivity measurements corresponding to an earlier time period (1980s and 1990s) than float profiles (2012 and beyond). We have made an effort to match as many float and observational profiles as possible within each region, but submesoscale variability can still lead to important discrepancies in productivity between profiles. Ideally, a formal validation exercise would include paired in situ ^{14}C incubations with biogeochemical and bio-optical profiles from BGC-Argo floats. A noteworthy takeaway from this qualitative analysis is that, on average, the CbPM$_{Argo}$ seems to replicate well the observed productivity profile whenever surface NPP conditions in the float data are similar to observations. Additionally, the vertical structure of the averaged productivity profiles derived from CbPM$_{Argo}$ show distinct regional features, in consonance with the in situ ^{14}C-based profiles. This qualitative agreement yields some confidence in the utility of NPP estimates derived from the combination of the CbPM and float data to assess the output of satellite-based productivity algorithms, as presented in the following sections.

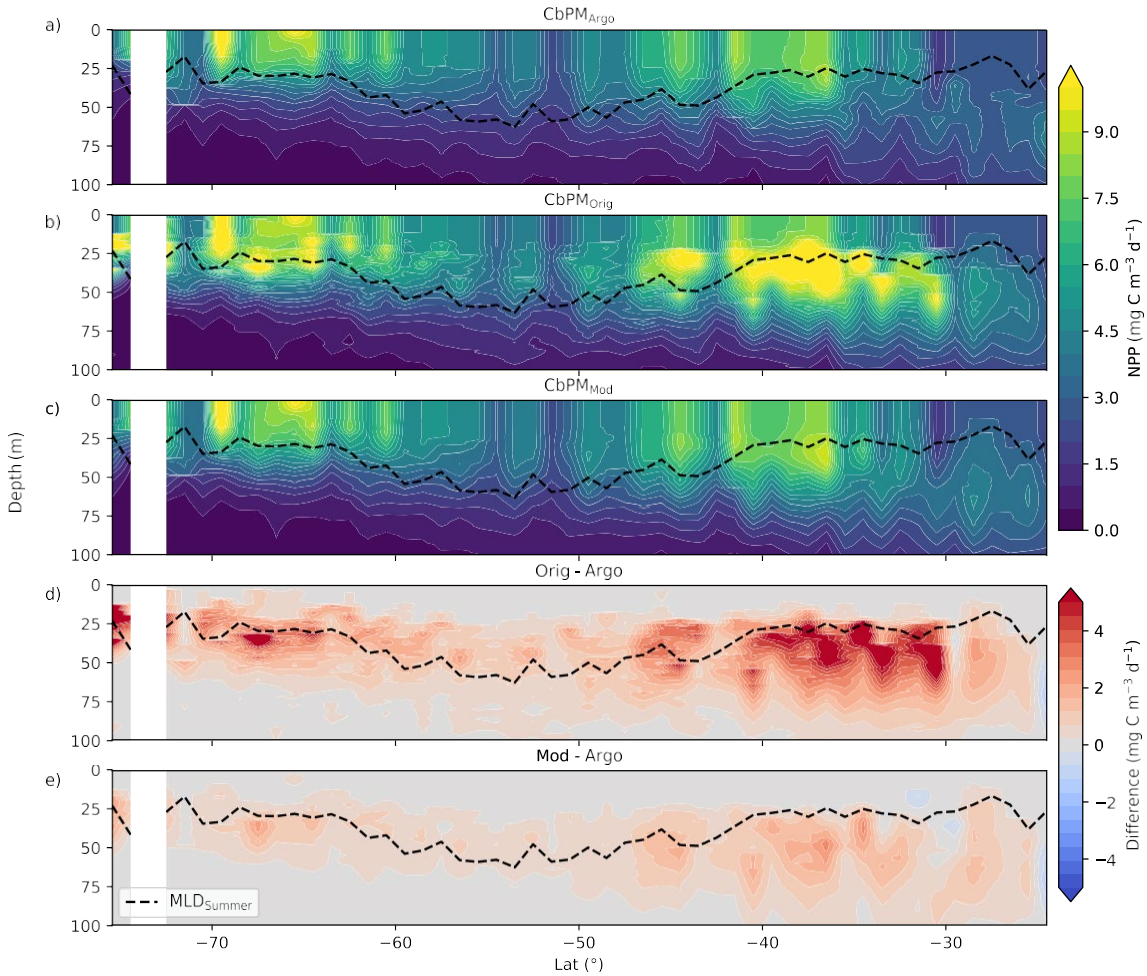

Figure 3. Zonally and seasonally averaged net primary production (NPP) (mg C m^{-3} d^{-1}) obtained from the (a) carbon-based productivity model (CbPM)$_{Argo}$, (b) CbPM$_{Orig}$, and (c) CbPM$_{Mod}$. (d) Difference in zonally and seasonally averaged NPP between the CbPM$_{Argo}$ and CbPM$_{Orig}$. (e) Difference in zonally and seasonally averaged NPP between the CbPM$_{Argo}$ and CbPM$_{Mod}$. NPP estimates were previously binned into a 1° by 1° grid.

3.2. Assessment of Vertically Resolved Output From CbPM Implementations in the Southern Ocean

3.2.1. NPP

We compare meridional sections in vertically resolved modeled NPP between the three model implementations (CbPM$_{Argo}$, CbPM$_{Orig}$, and CbPM$_{Mod}$) within the Southern Ocean. We focus on the Southern Ocean as this region has the highest density of BGC-Argo floats with paired biogeochemical and bio-optical profiles in the global ocean. The Southern Ocean is, nonetheless, a challenging region in which to interpret the inferred vertical structure in phytoplankton growth and productivity by the CbPM. As mentioned above, the original satellite application of this model was not developed to account for iron limitation, a scarce nutrient in most of the non-coastal Southern Ocean (Martin et al., 1990; Moore et al., 2013). The most relevant features in depth-resolved NPP are observed in the upper 100 m in all three model implementations (Figures 3a–3c). Zonally averaged estimates of vertically resolved NPP from the three model implementations show some common characteristics, such as higher NPP rates between 45°S and 30°S and south of 60°S (Figures 3a–3c). Depth-resolved NPP is lower across model configurations roughly between 45°S and 60°S, where the lowest iron concentrations are observed on average for the Southern Ocean (Arteaga et al., 2019; Tagliabue et al., 2012). The overall range and meridional gradient in vertically resolved NPP is similar to that observed in zonally averaged ^{14}C incubations (Buitenhuis et al., 2013). Float data latitudinally spread across the Southern Ocean is available for all seasons, with at least (and often more than) one full annual cycle of profiles (minimum of 4 profiles per month during 12 consecutive months). Zonally

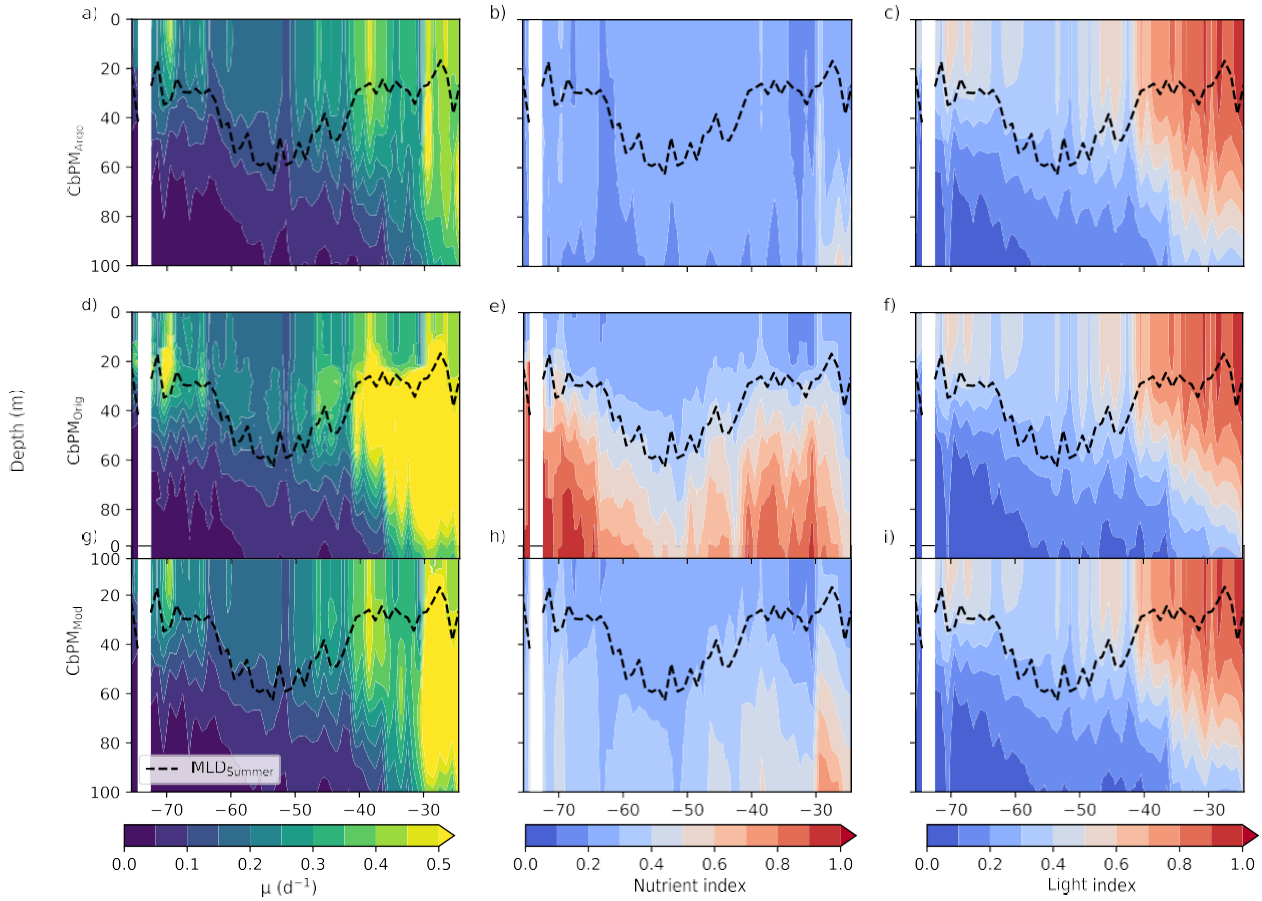

Figure 4. Zonally and seasonally averaged phytoplankton (a) division rate (μ, d^{-1}), (b) nutrient index (unitless), and (c) light index (unitless) inferred by the carbon-based productivity model (CbPM)$_{Argo}$. Panels (d–f) show the same variables inferred by the CbPM$_{Orig}$. Panels (g–i) show the same variables inferred by the CbPM$_{Mod}$. All variables were previously binned into a 1° by 1° grid.

averaged outputs in polar latitudes from the CbPM have a slight bias toward high light months imposed by the inability to compute NPP when the solar zenith angle exceeds 90° (due to unavailable PAR retrievals).

Across depth, the largest discrepancies between model implementations are observed below the summer MLD (Figures 3d and 3e). Both, CbPM$_{Orig}$, and CbPM$_{Mod}$, tend to overestimate NPP at depth with respect to the CbPM$_{Argo}$. The CbPM$_{Orig}$ shows a higher positive bias in productivity with respect to the CbPM$_{Argo}$, with depth-resolved differences >4 mg C m^{-3} d^{-1} (Figure 3d). This represents about 50% of the highest zonally averaged NPP computed by the CbPM$_{Argo}$. The positive bias in NPP by the CbPM$_{Mod}$ is lower and constrained to ~2 mg C m^{-3} d^{-1}. The only distinction in the configuration of the CbPM$_{Mod}$ and CbPM$_{Orig}$ south of 30°S, is that the CbPM$_{Mod}$ uses ferricline instead of nitracline to parameterize photoacclimation. It is important to note that differences between model implementations are always only obtained below the averaged local mixed layer, given that for this comparison, input variables have been averaged within the mixed layer in all three implementations.

3.2.2. Division Rate, Nutrient and Light Index

Similarly as for NPP, large discrepancies in phytoplankton growth parameters (μ, nutrient and light indices) between model implementations are observed at depth in the Southern Ocean (Figure 4). The CbPM$_{Argo}$ shows highest division rates near the surface and decreasing with depth (Figure 4a), except north of 30°S, where deep light penetration permits the increase of division rates below the summer mixed layer (Figure 4c). High NPP rates in subsurface waters derived from the CbPM$_{Orig}$ are a consequence of very high subsurface phytoplankton division rates predicted in this implementation (Figure 4d). Here, inferred μ north of 40°S and below the summer

mixed layer is >0.5 days^{-1}, higher than predicted by the CbPM$_{Argo}$ and CbPM$_{Mod}$ (Figures 4a and 4g). This is driven by the high nutrient and light indices modeled (reconstructed) in the CbPM$_{Orig}$ (Figures 4e and 4f). A high nutrient index signifies nutrient saturation, while a low nutrient index indicates nutrient limitation of phytoplankton growth. The CbPM$_{Orig}$ predicts a substantial relaxation in nutrient stress below the summer mixed layer across the entire Southern Ocean (i.e., nutrient index >0.5). By substituting the nitracline depth for the ferricline to constrain nutrient limitation, the CbPM$_{Mod}$ is able to produce a nutrient index (limitation) pattern more in accordance to what predicted by the CbPM$_{Argo}$ (Figures 4h and 4b), which is constrained by the local Chl:C inferred from the floats, and more in line with what expected from severe iron limitation of phytoplankton growth diagnosed in this region (Boyd et al., 2007; Martin et al., 1990). By placing the ferricline at a depth of 333 m we effectively impose severe nutrient limitation on the photoacclimation scheme of the CbPM$_{Mod}$. The ferricline depth horizon at 333 m was chosen based on the analysis of in situ iron data in the Southern Ocean (Tagliabue et al., 2014). The photoacclimation nutrient stress term of the original CbPM responds to Δz_{NO3}, which is the depth difference between a given parcel of water and the nitracline (or ferricline in this case). Based on the analysis of the photoacclimation nutrient stress term (Figure 1), any depth difference (Δz) ≥ 100 m will already impose the maximum possible photoacclimation nutrient stress in the model. The strong nutrient stress imposed by the ferricline south of 30°S is evident near 100 m in the CbPM$_{Mod}$ (Figure 4h). South of 30°S, high nutrient limitation results in a low nutrient index (blue colors), while north of this latitude, nutrient limitation is drastically relaxed yielding a high nutrient index (red colors).

The phytoplankton growth light level index is very similar between all three model implementations (Figures 4c, 4f and 4i). As explained above, phytoplankton growth parameters (and resulting NPP) for this comparison are computed by averaging phytoplankton biomass properties within the mixed layer in all three model implementations. Thus, the resulting light attenuation within the mixed layer, where planktonic biomass tends to be highest, is the same in all model implementations leading to very similar patterns in the zonally averaged light index profile. Small differences can still exist at depth due to differences in the subsurface reconstruction of biomas between model implementations.

3.2.3. Phytoplankton Biomass and Chl:C Ratio

The disagreement in productivity estimates between model implementations is fundamentally driven by differences between the float Chl:C ratio used as input in the CbPM$_{Argo}$ (Figure 5a), and the inferred vertical profiles of Chl:C derived from the CbPM$_{Orig}$ (Figure 5d) and CbPM$_{Mod}$ (Figure 5g). In the Southern Ocean, the float data driving the CbPM$_{Argo}$ shows mostly a constant Chl:C in the first 100 m. Meanwhile, the zonally averaged Chl:C ratio inferred (reconstructed) by the CbPM$_{Orig}$ shows a clear increase with depth, particularly below the summer mixed layer. The CbPM$_{Mod}$ output also shows an increase in Chl:C with depth, but this is less pronounced than in the CbPM$_{Orig}$.

In terms of biomass estimated from the floats bio-optical instruments, water column sections with high chlorophyll concentration mostly coincide with sections with high phytoplankton carbon biomass (C_{phyto}) (Figures 5b and 5c). The strong increase in phytoplankton Chl:C with depth predicted by the CbPM$_{Orig}$ results in "artificially" high subsurface chlorophyll levels, particularly below the summer mixed layer (Figure 5e), not observed in the float data. The less severe increase in Chl:C with depth predicted by the CbPM$_{Mod}$ (Figure 5g) results in a less pronounced subsurface chlorophyll maxima in the Southern Ocean (Figure 5h), which is still unrealistic when compared with the zonally averaged float data in this region.

Highest zonally averaged float C_{phyto} is observed in latitudes <60°S (Figure 5c). To enforce consistency in the evaluation of output from all three model implementations, zonally averaged data for all three implementations includes only profiles that have valid PAR matchups and permit the reconstruction of the vertical profile in C_{phyto} and Chl by the CbPM$_{Orig}$ and CbPM$_{Mod}$. Therefore, the spatial pattern in C_{phyto} observed in the float data forcing the CbPM$_{Argo}$ might reflect a slight bias toward high light periods (zenith angle >90°) at higher latitudes. The zonally averaged pattern in C_{phyto} is very similar between the float profiles used to inform the CbPM$_{Argo}$ and the vertical profiles inferred by the CbPM$_{Orig}$ and CbPM$_{Mod}$ (Figures 5c, 5f and 5i). This suggests that deficiencies in the estimation of vertically resolved productivity by the CbPM$_{Orig}$ (and to a lesses extent, by CbPM$_{Mod}$) in the Southern Ocean with respect to the CbPM$_{Argo}$ are related to the modeling of the Chl:C ratio with depth as a consequence of photoacclimation and not the inference of phytoplankton carbon biomass.

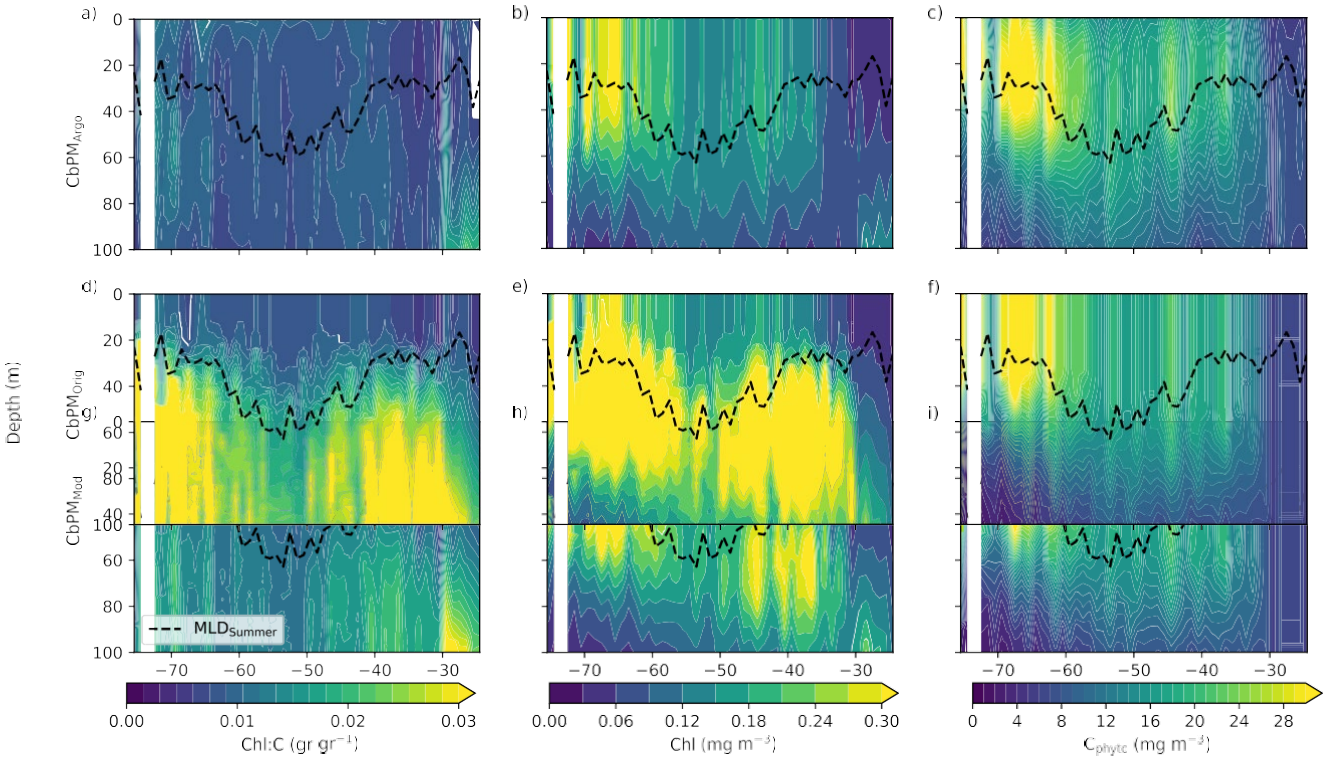

Figure 5. Zonally and seasonally averaged phytoplankton (a) Chl:C ratio (gr gr^{-1}), (b) Chl (mg m^{-3}), and (c) C_{phyto} (mg m^{-3}) used by the carbon-based productivity model (CbPM)$_{Argo}$. Panels (d–f) show the same variables inferred by the CbPM$_{Orig}$. Panels (g–i) show the same variables inferred by the CbPM$_{Mod}$. All variables were previously binned into a 1° by 1° grid.

3.2.4. Photoacclimation and Float-Based Chl Driving the CbPM

The CbPM describes the physiological state of phytoplankton cells expressed through variations in their Chl:C ratio. NPP and μ are parameterized as a function of cellular Chl:C and its response to changes in ambient nutrient (nitrogen) and light, where nutrient stress is inferred from the vertical distance between a given water parcel and the nitracline (assuming the latter one is deeper, Westberry et al., 2008). The CbPM was originally developed to reproduce vertical profiles of productivity and phytoplankton biomass in nitrate limited oligotrophic waters. The oceanic region around the Hawaii Ocean Time-series has the advantage of presenting conditions similar to those targeted by the original CbPM, and it has a field sampling program with a large record of depth-resolved ^{14}C-based productivity and fluorometric chlorophyll measurements taken at station ALOHA (Karl et al., 2021). Additionally, bio-optical float profiles for all seasons are available nearby station ALOHA, allowing us to compare float productivity and Chl profiles with in situ data from different periods of the annual cycle (Figure 6). Float-based output from all three model implementations (CbPM$_{Argo}$, CbPM$_{Orig}$, and CbPM$_{Mod}$) show a similar productivity profile of low surface NPP and increased productivity below the mixed layer, followed by NPP attenuation with depth (Figure 6, left panels). Float-based NPP agree within the uncertainty with in situ productivity measurements below the mixed layer, but show a large discrepancy at surface, where in situ observations exhibit higher NPP rates than those yielded by the float-based estimates. We investigate whether this inconsistency is rooted in the float-based surface Chl estimate by computing satellite-informed productivity profiles from the CbPM$_{Sat}$. The magnitude of surface NPP by the CbPM$_{Sat}$ is greater than the float-based estimates and in better agreement with observations (Figure 6, dashed blue line). Surface Chl estimates by the CbPM$_{Sat}$ are also within the uncertainty of observations, but yield a higher subsurface Chl maximum below the mixed layer (Figure 6, right panels). Mean float-based surface Chl concentrations underestimate observations, similarly as for NPP rates. This suggests that

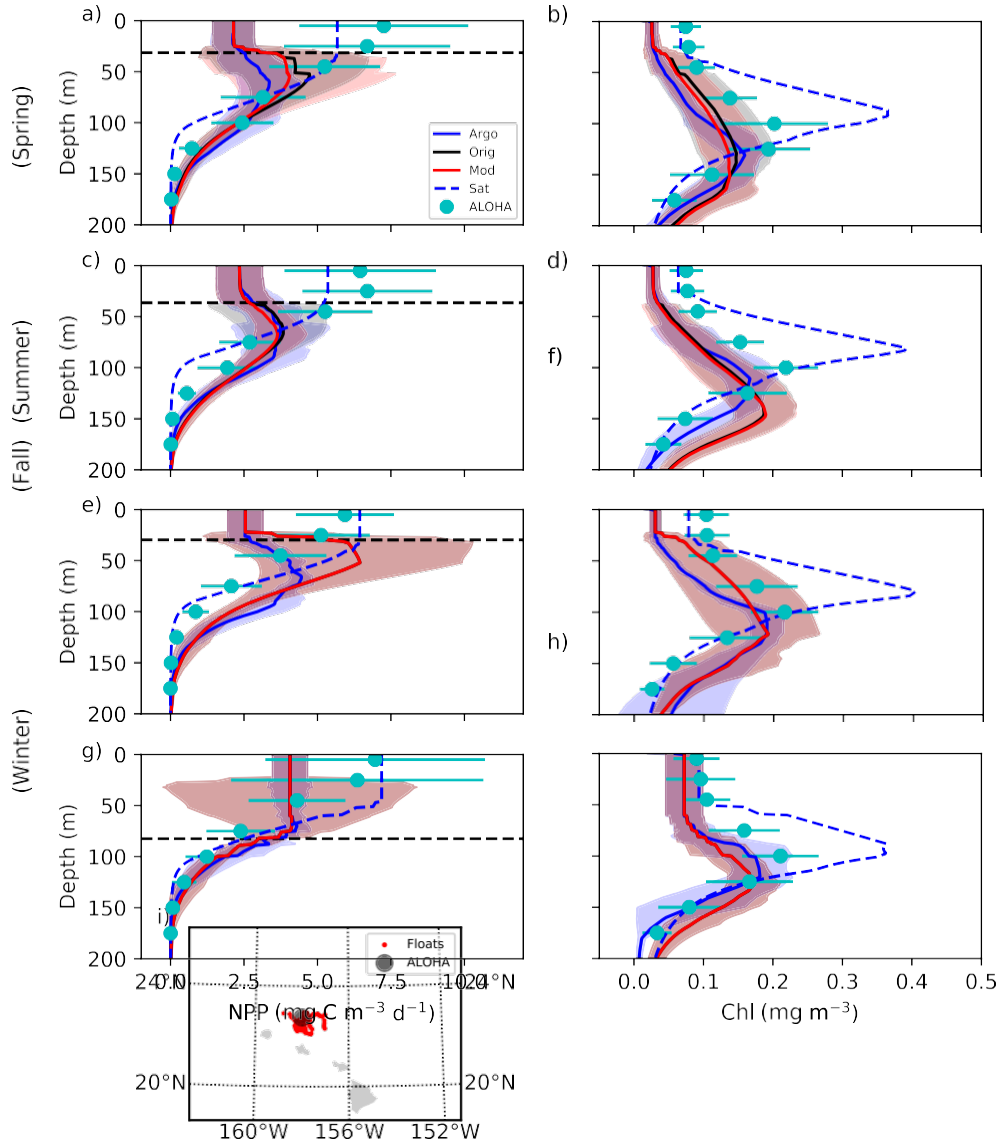

Figure 6. Seasonally averaged net primary production (mg C m^{-3} d^{-1}) (left column) and Chl (mg C m^{-3}) (right column) profiles near station ALOHA for (a–b) Spring, (c–d) Summer (e–f) Fall, (g–h) Winter (boreal seasons). Profiles are obtained from the carbon-based productivity model $(CbPM)_{Argo}$ (Argo, solid blue line), $CbPM_{Orig}$ (Orig, solid black line), $CbPM_{Mod}$ (Mod, solid red line), $CbPM_{Sat}$ (Sat, dashed blue line), and in situ observations (ALOHA, solid cyan circles ± standard deviation). Shaded areas represent ± standard deviation of the float-based model implementations. Horizontal dashed black line represents average mixed layer depth. (i) Location of float profiles (red) and in situ field station (dark gray).

deficiencies in float-based surface productivity nearby ALOHA might indeed be related to problems with the estimation of surface Chl by the floats in this region. We hypothesize that potentially biased-low float Chl estimates at ALOHA could be due to the applied fluorescence quenching correction which was developed in Southern Ocean waters and might not be entirely applicable in subtropical regions (Xing et al., 2012). We do not expect this issue to affect productivity profiles in the Southern Ocean since previous analyses indicate a good agreement between fluorescence-based float Chl and satellite ocean color data in this region (Haëntjens et al., 2017).

Mean float-based surface estimates of C_{phyto} are slightly lower than observations at station ALOHA, but agree within the uncertainty range (Figure S3 in Supporting Information S1, right panels). The overall mean vertical profile in float-based C_{phyto} is similar to that of observations in all seasons. Satellite-based estimates of C_{phyto} from the $CbPM_{Sat}$ are greater that observations and float-based profiles, especially in the upper 100 m. The vertical pattern in Chl:C derived from the float bio-optical sensors ($CbPM_{Argo}$) at station ALOHA agrees reasonably well with that derived from Chl and C_{phyto} observations, as well as the average profile reconstructed by the float-based ($CbPM_{Orig}$ and $CbPM_{Mod}$) and satellite ($CbPM_{Sat}$) model implementations (except for winter, where $CbPM_{Sat}$ underestimate other surface estimates) (Figure S3 in Supporting Information S1, left panels). In all cases, the Chl:C ratio increases with depth to about 100 m or deeper. Below the maximum Chl:C depth, the Chl:C observed in the Argo float data (Figure S3 in Supporting Information S1, solid blue line) and that inferred from in situ biomass observations (Figure S3 in Supporting Information S1, solid cyan circles) start to decrease due to degradation of the photosynthetic pigments associated with cellular death (Veldhuis et al., 2001), while the fully reconstructing implementations of the CbPM do not account for this degradation and maintain the high Chl:C ratio achieved via the model's parameterization of photoacclimation (Figure S3 in Supporting Information S1). Our initial conclusion from this comparison exercise at station ALOHA is that errors in surface estimates of phytoplankton biomass, particularly Chl, by the float bio-optical sensors can bias float-based surface NPP rates derived from the CbPM (Long et al., 2021), but the model is able to rectify the estimation of productivity at depth by inferring the correct Chl:C ratio resulting from the photoacclimation scheme.

Contrary to what is observed at station ALOHA, in the Southern Ocean the $CbPM_{Orig}$ fails to reproduce the depth-resolved patterns of NPP inferred by the float-data-driven $CbPM_{Argo}$ (Figure 3). The disagreement is largest during summer, where the $CbPM_{Orig}$ predicts a pronounced subsurface increase in NPP missing in the $CbPM_{Argo}$ output, which shows a monotonic decline in NPP below the mixed layer (Figure 7, left panels). Similarly as for NPP, the $CbPM_{Orig}$ depicts a substantial increase in Chl with depth not observed in the float data ($CbPM_{Argo}$) (Figures 5 and Figure 7, right panels). The $CbPM_{Mod}$, which differs from the $CbPM_{Orig}$ in that it uses a constant ferricline instead of nitracline to parameterize productivity profiles south of 30°S, yields NPP rates and Chl estimates closer to the $CbPM_{Argo}$ albeit a reduced increase in subsurface productivity and Chl (Figure 7). As discussed above, imposing the ferricline at 333 m (Tagliabue et al., 2014) effectively enhances nutrient stress in the model and down-regulates photoacclimation of the Chl:C ratio.

Seasonally averaged profiles of C_{phyto} agree within the uncertainty for the three float-based model implementations (Figure S4 in Supporting Information S1, right panels). However, seasonally averaged profiles of Chl:C diverge, where float data ($CbPM_{Argo}$) exhibit a mostly constant Chl:C ratio throughout the water column, while the Chl:C ratio inferred by the $CbPM_{Orig}$ primarily increases with depth (Figure S4 in Supporting Information S1, left panels). This vertical pattern in Chl:C suggests a lack of photoacclimation with depth by Southern Ocean phytoplankton communities. This is somewhat of a surprising result since phytoplankton in the laboratory have been shown to employ strategies to maintain high pigment levels under low iron-low light conditions (Strzepek et al., 2012). One such strategy is an increase in the size of photosynthetic units (PSUs) accomplished through higher amounts of light-harvesting pigments and their arrangement (Strzepek et al., 2012). This acclimation strategy does not increase cellular iron requirements. A muted photoacclimation response is not only observed in vertical profiles, but also in the relationship of the Chl:C against the median mixed layer light level (Figure S5 in Supporting Information S1), where data for the Southern Ocean fail to show the pronounced increase in Chl:C at low mixed layer light levels observed for other latitudes. If phytoplankton communities in the Southern Ocean are indeed limited in their photoacclimation capacity due to iron stress, the mechanistic argument by which the $CbPM_{Mod}$ achieves a better agreement with float Chl:C data and NPP estimates from the $CbPM_{Argo}$ compared to $CbPM_{Orig}$ would be valid. That is, a deep ferricline would impose severe nutrient stress on phytoplankton physiology, impeding photoacclimation (Geider & LaRoche, 1994). In contrast to the laboratory results described above, the muted increase in Chl:C observed in our field float data below the mixed layer suggests that a further expansion in PSU size is not a viable strategy for responding to decreasing light levels with increasing depth. Accordingly, photoacclimation at these depths would require an increase in the number of PSUs, with an associated rise in cellular iron demands difficult to meet in an environment with such deep ferricline and limited external iron inputs (Tagliabue et al., 2014).

A potential alternate explanation is that photoacclimation of Southern Ocean phytoplankton with depth is being masked by the presence of disconnected light-harvesting complexes (DLHCs) in surface populations (Behrenfeld

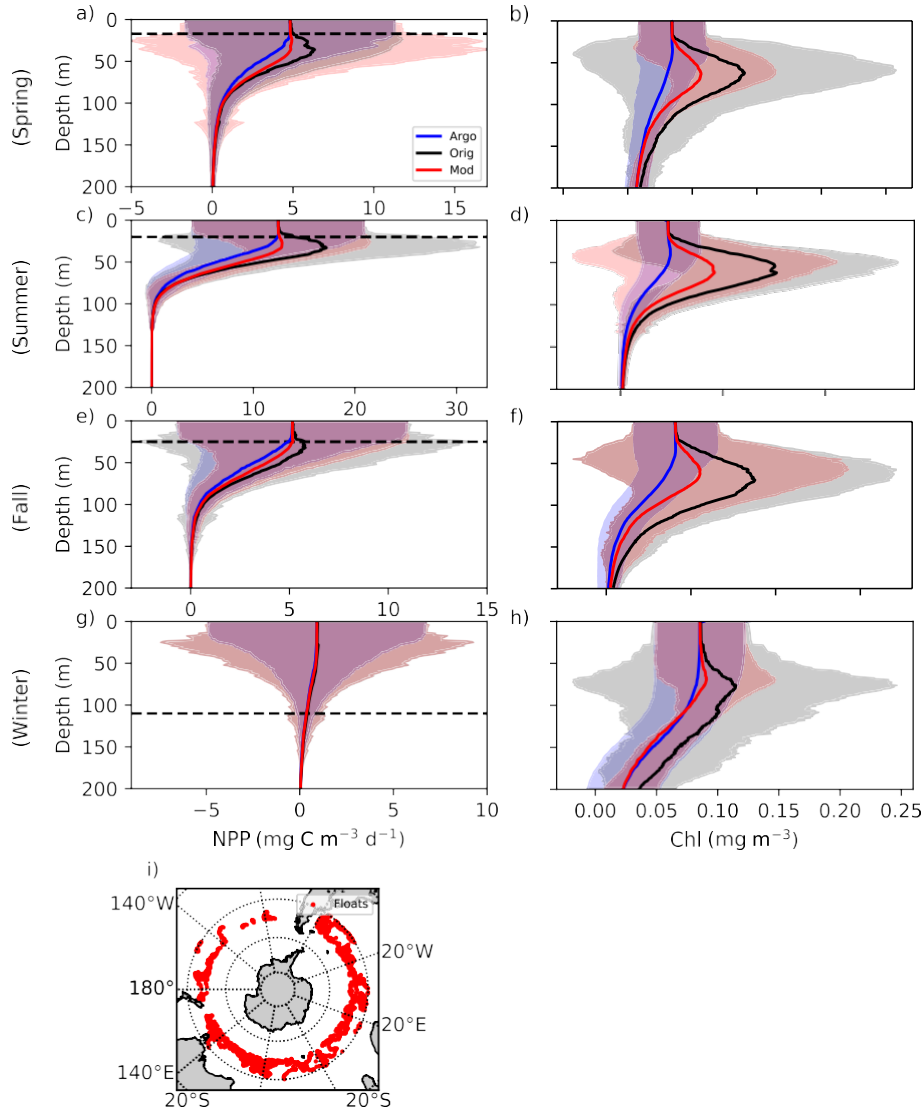

Figure 7. Seasonally averaged net primary production (mg C m^{-3} d^{-1}) (left column) and Chl (mg C m^{-3}) (right column) profiles in the Southern Ocean between 40°S and 50°S for (a–b) Spring, (c–d) Summer (e–f) Fall, (g–h) Winter (austral seasons). Productivity profiles are obtained from the carbon-based productivity model $(CbPM)_{Argo}$ (Argo, solid blue line), $CbPM_{Orig}$ (Orig, solid black line), and $CbPM_{Mod}$ (Mod, solid red line). Shaded areas represent ± standard deviation of the float-based model implementations. Horizontal dashed black line represents average mixed layer depth. (i) Location of float profiles (red).

& Milligan, 2013, and references therein). DLHCs are uncoupled pigment proteins that can accumulate in phytoplankton under conditions of iron stress in the presence of elevated macronutrients (Behrenfeld et al., 2006; Schrader et al., 2011), which is the common condition of Southern Ocean waters. In some phytoplankton species (*Chlamydomonas reinhardtii*) evidence of DLHCs has been found even before iron-stress chlorosis has been induced (Moseley et al., 2002). These pigment proteins are fluorescence-emitting, and hence, would not be distinguishable from chlorophyll in functional pigment proteins *a* by the bio-optical sensors on board BGC-Argo floats.

3.3. Meridional Variability of the Base of the Productive Layer Inferred From the $CbPM_{Argo}$

We explore next one of the potential applications of having depth-resolved productivity estimates across different regions of the global ocean. We analyze meridional variations in the depth of the productive layer and how it compares with variations in metrics commonly used to define the surface most productive region of the ocean,

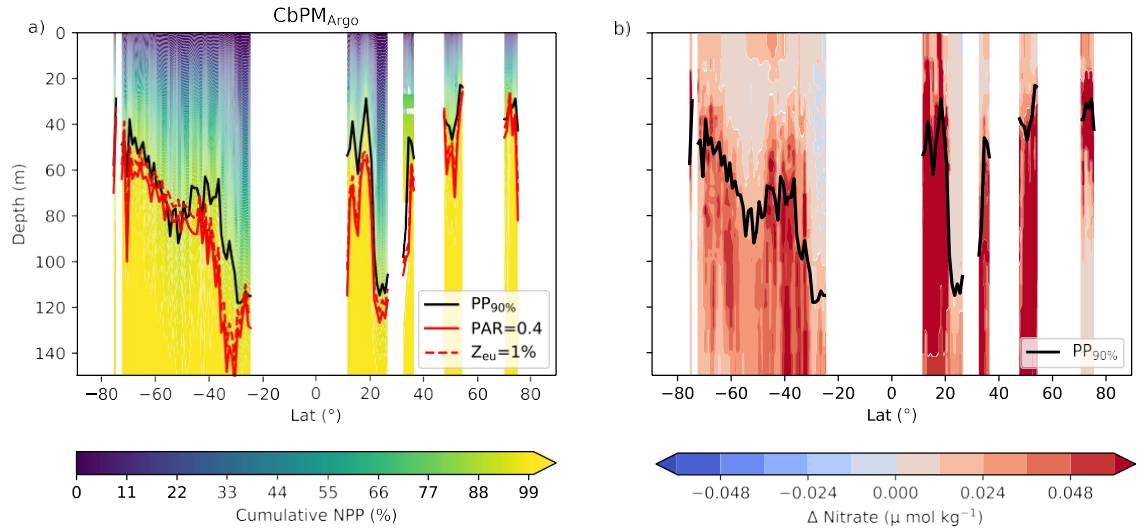

Figure 8. (a) Zonally and seasonally averaged depth-cumulative net primary production (%) inferred by the carbon-based productivity model (CbPM) $_{Argo}$. (b) Vertical gradient (Δ) in the nitrate concentration (μ mol kg^{1}) computed from zonally and seasonally averaged nitrate profiles measured by the floats. The black line in both panels represents the depth above which 90% of vertical productivity has occurred (PP$_{90\%}$). The solid red line in (a) represents the constant isolume depth defined at PAR = 0.4 (E m $^{-2}$ d $^{-1}$). The dashed red line in (a) represents the euphotic depth (Z$_{eu}$) defined at the 1% fraction of surface PAR.

such as euphotic depth and isolume. We operationally define the base of the productive layer as the depth above which 90% of vertically integrated productivity has occurred (PP$_{90\%}$). Euphotic depth (Z$_{eu}$) is defined as the depth at which PAR is 1% of that at the surface. The isolume is defined as the depth where PAR = 0.4 E m $^{-2}$ d $^{-1}$. The isolume depth and Z$_{eu}$ are obtained based on the zonally and temporally averaged gridded PAR field from the spectral component of the CbPM$_{Argo}$. We base this analysis on output from the CbPM$_{Argo}$ since it is guided by float-based Chl:C to constrain photoacclimation, division rates, and NPP. Here, we also include data beyond the Southern Ocean in order to compute zonal averages, but it is important to highlight that data in the northern hemisphere are only truly representative of specific regions such as the western and central North Pacific, the Sub-Arctic North Atlantic, and the Arabian Sea.

The meridional variability in PP$_{90\%}$ mirrors that of the Z$_{eu}$ and isolume (Figure 8a). Previous work conducted in the North Pacific subtropical gyre has shown covariability in the depth displacement of the isolume (defined at ~ PAR = 0.4 E m $^{-2}$ d $^{-1}$) and the vertical position of the nitracline (defined as the shallowest depth at which the NO_3^- + NO_2^- depth gradient exceeds 2 nmol kg^{-1} m^{-1}, Letelier et al., 2004). We investigate this relationship by computing the vertical gradient in zonally averaged paired nitrate profiles obtained from the BGC-Argo floats. Overall, we find similar meridional covariability between the depth displacement of PP$_{90\%}$, Z$_{eu}$, isolume, and the shallowest depth at which relatively strong vertical nitrate gradients begin to occur in the water column (Δ Nitrate, where positive values represent higher nitrate concentration toward depth) (Figure 8b). It is somewhat surprising that these depth horizons agree well even in the Southern Ocean where nitrate is not considered the primary limiting nutrient (Moore et al., 2013). Our initial interpretation is that biomass shading and decrease in PAR with depth mostly dictate the overall vertical extent of the productive layer and determine the depletion depth of nutrients that tend to be well mixed in the upper ocean such as nitrate. However, depth resolved information on other nutrients such as phosphate and iron would help to validate this interpretation. It is important to note that the CbPM$_{Argo}$ is not informed by float nitrate information, and thus, the similarity in the meridional pattern of PP$_{90\%}$ and that of the inferred shallow nitracline is an emergent outcome that results from the variability in float-based biomass and Chl:C ratio driving NPP in the CbPM$_{Argo}$.

3.4. Differences in Vertically Integrated NPP

Global patterns in vertically integrated NPP obtained from the individual productivity profiles derived from the CbPM$_{Argo}$ (Figure 9) show mean seasonal variability in high latitude (roughly >45°) net carbon fixation between <100 and >800 mg C mg^{-2} d^{-1} from winter to summer, and intermediate values in mid-latitudes (25°–45°) between 300 and 500 mg C m^{-2} d^{-1}, consistent with the range in depth-integrated productivity observed in

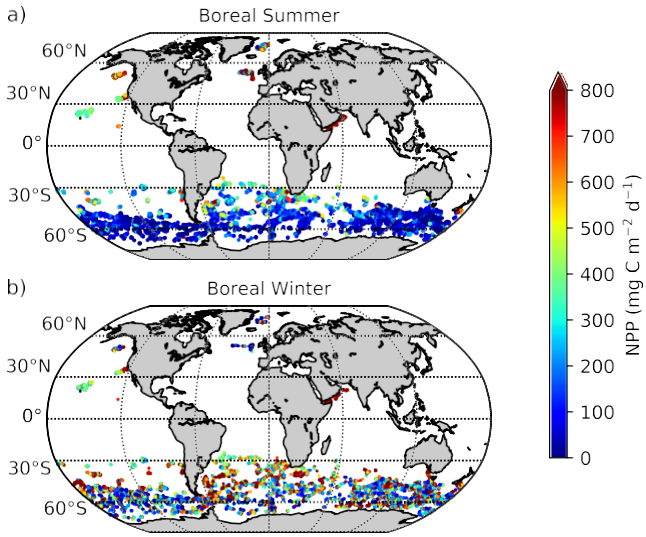

Figure 9. Global patterns in float-based vertically integrated net primary production (mg C m^{-2} d^{-1}) obtained by the carbon-based productivity model$_{Argo}$ averaged for (a) boreal spring and summer months (April–September) and (b) boreal fall and winter months (October–March).

satellite-based and general circulation models (GCMs) (Carr et al., 2006). Global patterns in vertically integrated NPP obtained from the CbPM$_{Orig}$ and CbPM$_{Mod}$ (not shown) are very similar to that of the CbPM$_{Argo}$, given that differences in vertically resolved NPP below the mixed layer occur at relatively low productivity levels which do not impact greatly depth-integrated estimates.

North of 30°S, estimates of vertically integrated NPP from the CbPM$_{Orig}$ correlate well with estimates from the CbPM$_{Argo}$, explaining >90% of the variability in float-based productivity (r^2 = 0.94, obtained from a type II linear model) (Figure 10a). The mean bias between these two model implementations is of 56 mg C^{-2} d^{-1}. The correction applied in the CbPM$_{Mod}$ to floats north of 30°S of defining the nitracline as the depth of maximum nitrate gradient in cases where the depth of nitrate >0.5 μ mol kg^{-1} is shallower than the depth of the mixed layer has a modest impact on vertically integrated NPP, improving r^2 between CbPM$_{Mod}$ and CbPM$_{Argo}$ to 0.96 and reducing the overall bias to 32 mg C^{-2} d^{-1} (Figure 10b).

South of 30°S, vertically integrated NPP from the CbPM$_{Orig}$ consistently overestimates output from the CbPM$_{Argo}$ (Figure 10c). This overestimation results from high NPP bellow the mixed layer predicted by the CbPM$_{Orig}$ driven by "artificially" high Chl:C ratios and division rates inferred by this model configuration (see discussion above). The mean bias between the

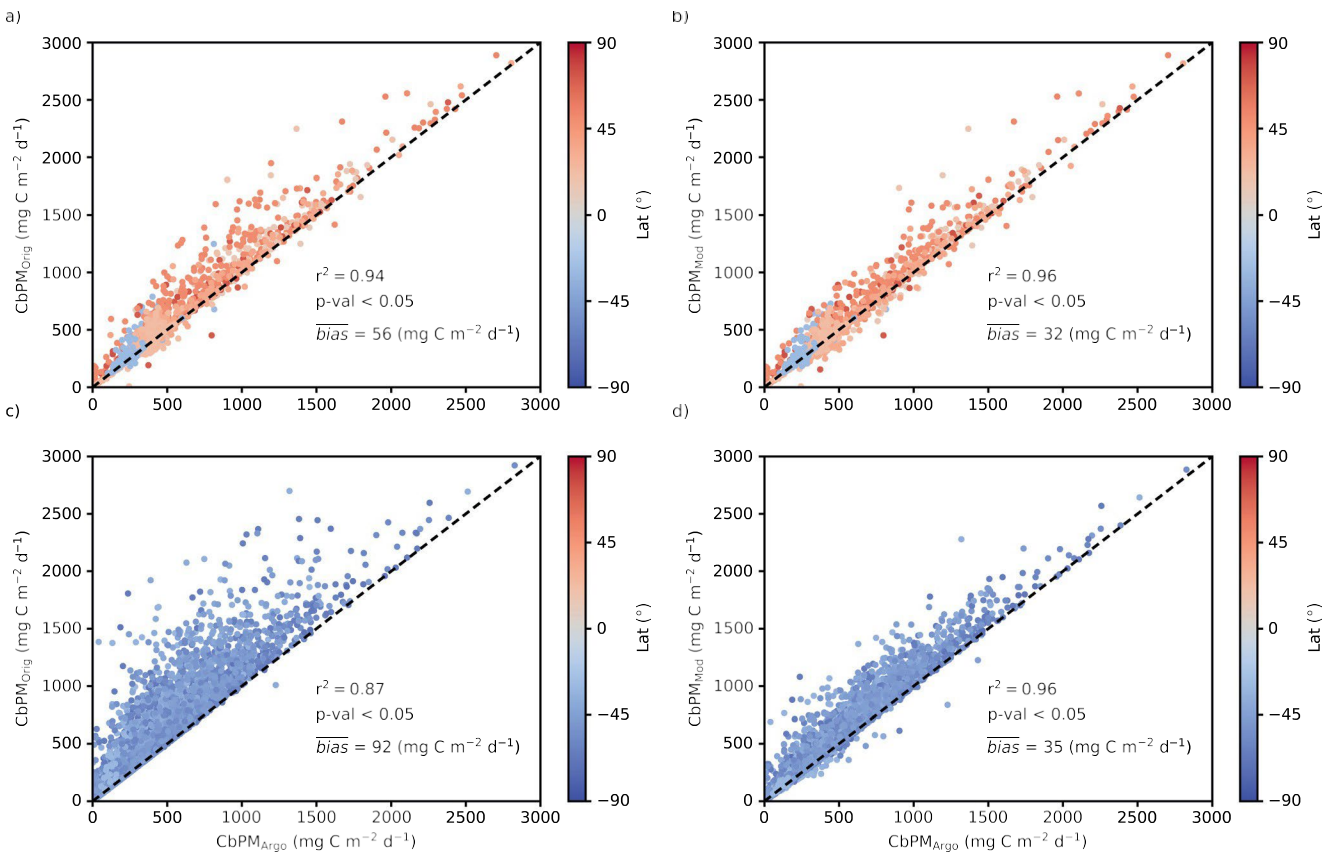

Figure 10. Scatterplots of vertically integrated net primary production (NPP) (mg C m^{-2} d^{-1}) obtained for profiles north of 30°S by the (a) carbon-based productivity model (CbPM)$_{Argo}$ versus CbPM$_{Orig}$, (b) CbPM$_{Argo}$ versus CbPM$_{Mod}$, and south of 30°S by the (c) CbPM$_{Argo}$ versus CbPM$_{Orig}$, (d) CbPM$_{Argo}$ versus CbPM$_{Mod}$. The coefficient of determination (r^2) and p-value are based on a type II linear regression fit. The mean bias ( ) is computed as the averaged difference between vertically integrated NPP estimates obtained from individual float-based productivity profiles.

$CbPM_{Orig}$ and $CbPM_{Argo}$ is 92 mg C^{-2} d^{-1}, with a r^2 = 0.87. Southern Ocean output in vertically integrated NPP from $CbPM_{Mod}$ agrees better with that of the $CbPM_{Argo}$, with a reduced mean bias of 35 mg C^{-2} d^{-1} and an improved r^2 of 0.96 (Figure 10d). This improvement is driven by the substitution of the nitracline depth for the ferricline in the computation of the photoacclimation nutrient stress in the $CbPM_{Mod}$.

4. Conclusions

We use BGC-Argo float data to inform a productivity model initially developed for satellite applications (CbPM) and compute depth-resolved NPP in regions with available biogeochemical and bio-optical profiles. The combination of the CbPM and depth-resolved Chl:C based on float data ($CbPM_{Argo}$) is able to replicate well the vertical structure in ^{14}C incubations observed in various ocean regions such as the Southern Ocean, the North Pacific Central Gyre, the Sub-Arctic North Atlantic, and the Arabian Sea.

Subsequently, we compare three different implementations of the CbPM where productivity estimates below the mixed layer are obtained based on (a) float bio-optical profiles ($CbPM_{Argo}$), (b) fully inferring phytoplankton biomass and Chl:C based on mixed layer properties using the nitracline as a proxy for vertical nutrient limitation ($CbPM_{Orig}$), and (c) substituting the nitracline for the ferricline in Southern Ocean waters (south of 30°S) ($CbPM_{Mod}$). The biomass reconstructing and nitracline-based $CbPM_{Orig}$ results in higher NPP estimates below the mixed layer when compared to output from the float-based $CbPM_{Argo}$ in the Southern Ocean. Unrealistic high NPP at depth is driven by "artificially" high modeled Chl:C ratios and division rates. The $CbPM_{Mod}$ yields lower NPP rates than the $CbPM_{Orig}$ and a closer agreement with the $CbPM_{Argo}$. Depth-resolved profiles of Chl and Chl:C inferred from the $CbPM_{Mod}$ are in better agreement with float bio-optical estimates than profiles derived from the $CbPM_{Orig}$, suggesting that accounting for deep nutrient (iron) stress impacts on photoacclimation can improve estimates of productivity from the CbPM in the Southern Ocean. An analysis of in situ observations of productivity as well as float- and satellite-based implementations of the CbPM at station ALOHA indicate that float fluorescence-based Chl estimates might be biased-low in this subtropical region, prompting a revision of the applicability of the applied quenching correction beyond Southern Ocean waters.

The meridional variability in the displacement of the base of the productive layer ($PP_{90\%}$) from the $CbPM_{Mod}$ agrees well with vertical changes in Z_{eu} and the isolume depth defined at PAR = 0.4 E m^{-2} d^{-1}. Changes in $PP_{90\%}$ mirror the meridional displacement in the shallowest depth at which relatively strong vertical nitrate gradients begin to occur in the water column. This is an emergent property of the $CbPM_{Argo}$, which is not informed by nitrate float information to model phytoplankton productivity. Differences in depth-resolved productivity between the three model implementations have a relatively modest impact on depth-integrated NPP. The largest difference is observed in the Southern Ocean (south of 30°S) between $CbPM_{Orig}$ and $CbPM_{Argo}$, with a mean positive bias of 92 mg C mg^{-2} d^{-1}. This bias is reduced by 62% in the $CbPM_{Mod}$ (35 mg C mg^{-2} d^{-1}) due to reduced NPP at depth predicted by this model implementation. Our results demonstrate that profiling data from BGC-Argo floats can serve to inform regional adjustments that lead to the improvement of productivity algorithms.

Data Availability Statement

BGC-Argo data were obtained from the SOCCOM program data portal: https://soccom.princeton.edu/content/data-access. Ocean color and surface light (PAR) data were obtained from the NASA Ocean Color website (https://oceancolor.gsfc.nasa.gov). Regional depth-resolved in situ ^{14}C-based NPP data were obtained from http://dmoserv3.bco-dmo.org/jg/serv/BCO-DMO/ISPP14C/c14_primary_prod.html0%7Bdir=dmoserv3.whoi.edu/jg/dir/BCO-DMO/ON_DEQUE3/,info=dmoserv3.bco-dmo.org/jg/info/BCO-DMO/ISPP14C/c14_primary_prod%7D. Data from station ALOHA were obtained via the Hawaii Ocean Time-series HOT-DOGS application (http://hahana.soest.hawaii.edu/hot/hot-dogs/), University of Hawaii at Manoa. National Science Foundation Award 1756517. The complete code for the original satellite-based CbPM is available at http://sites.science.oregonstate.edu/ocean.productivity/cbpm2.code.php. The adapted code used in the $CbPM_{Argo}$ to compute depth-resolved NPP based on float-derived Chl and C_{phyto} profiles is available at https://zenodo.org/record/6599224#23.YqJZFC1h3uM.

Acknowledgments
This work was supported by the National Aeronautics and Space Administration (NASA) award NNX17AI73G, the Southern Ocean Carbon and Climate Observations and Modeling (SOCCOM) program under the National Science Foundation (NSF) Award PLR-1425989, the NASA North Atlantic Aerosol and Marine Ecosystem Study (NAAMES, award NNX15AF30G), and the NASA EXport Processes in the Ocean from RemoTe Sensing (EXPORTS) study (Grant 80NSSC17K0568).

References

Arteaga, L. A. (2022). *CbPM for BGC-Argo floats*. Zenodo. https://doi.org/10.5281/zenodo.6599224

Arteaga, L. A., Boss, E., Behrenfeld, M. J., Westberry, T. K., & Sarmiento, J. L. (2020). Seasonal modulation of phytoplankton biomass in the Southern Ocean. *Nature Communications*, *11*(1), 5364. https://doi.org/10.1038/s41467-020-19157-2

Arteaga, L. A., Pahlow, M., Bushinsky, S. M., & Sarmiento, J. L. (2019). Nutrient controls on export production in the southern ocean. *Global Biogeochemical Cycles*, *33*(8), 942–956. https://doi.org/10.1029/2019GB006236

Banse, K. (1991). Rates of phytoplankton cell division in the field and in iron enrichment experiments. *Limnology & Oceanography*, *36*(8), 1886–1898. https://doi.org/10.4319/lo.1991.36.8.1886

Barber, R. T., Borden, L., Johnson, Z., Marra, J., Knudson, C., & Trees, C. C. (1997). Ground truthing modeled k_{PAR} and on deck primary productivity incubations with in-situ observations. In S. G. Ackleson & R. J. Frouin (Eds.), *Ocean optics XIII* (Vol. 2963, pp. 834–839). SPIE. https://doi.org/10.1117/12.266409

Barber, R. T., Marra, J., Halpern, D., Bidigare, R. R., Smith, S. L., Johnson, Z., et al. (2001). Primary productivity and its regulation in the Arabian Sea during 1995. *Deep-Sea Research II*, *48*(6–7), 1127–1172. https://doi.org/10.1016/s0967-0645(00)00134-x

Behrenfeld, M. J., Boss, E., Siegel, D. A., & Shea, D. M. (2005). Carbon-based ocean productivity and phytoplankton physiology from space. *Global Biogeochemical Cycles*, *19*(1), GB1006. https://doi.org/10.1029/2004GB002299

Behrenfeld, M. J., & Milligan, A. J. (2013). Photophysiological expressions of iron stress in phytoplankton. *Annual Review of Marine Science*, *5*(1), 217–246. https://doi.org/10.1146/annurev-marine-121211-172356

Behrenfeld, M. J., Worthington, K., Sherrell, R. M., Chavez, F. P., Strutton, P., McPhaden, M., & Shea, D. M. (2006). Controls on tropical Pacific Ocean productivity revealed through nutrient stress diagnostics. *Nature*, *442*(7106), 1025–1028. https://doi.org/10.1038/nature05083

Bleck, R. (2002). An oceanic general circulation model framed in hybrid isopycnic-Cartesian coordinates. *Ocean Modelling*, *4*(1), 55–88. https://doi.org/10.1016/S1463-5003(01)00012-9

Boss, E., & Behrenfeld, M. (2010). In situ evaluation of the initiation of the North Atlantic phytoplankton bloom. *Geophysical Research Letters*, *37*(18), L18603. https://doi.org/10.1029/2010GL044174

Boss, E., & Haëntjens, N. (2016). *Primer regarding measurements of chlorophyll fluorescence and the backscattering coefficient with WETLabs FLBB on profiling floats* (Technical Report No. SOCCOM Technical Report 2016-1). National Science Foundation Polar Programs PLR-1425989, NASA Earth Science NNX14AP49G. Retrieved from http://soccom.princeton.edu/sites/default/files/files/SOCCOM_2016-1_Bio-optics-primer.pdf

Boyd, P. W., Jickells, T., Law, C. S., Blain, S., Boyle, E. a., Buesseler, K. O., et al. (2007). Mesoscale iron enrichment experiments 1993–2005: Synthesis and future directions. *Science*, *315*(5812), 612–617. https://doi.org/10.1126/science.1131669

Buitenhuis, E. T., Hashioka, T., & Quéré, C. L. (2013). Combined constraints on global ocean primary production using observations and models. *Global Biogeochemical Cycles*, *27*(3), 847–858. https://doi.org/10.1002/gbc.20074

Carr, M., Friedrichs, M., Schmeltz, M., Noguchiaita, M., Antoine, D., Arrigo, K., et al. (2006). A comparison of global estimates of marine primary production from ocean color. *Deep Sea Research Part II: Topical Studies in Oceanography*, *53*(5–7), 741–770. https://doi.org/10.1016/j.dsr2.2006.01.028

Chai, F., Johnson, K. S., Claustre, H., Xing, X., Wang, Y., Boss, E., et al. (2020). Monitoring ocean biogeochemistry with autonomous platforms. *Nature Reviews Earth & Environment*, *1*(6), 315–326. https://doi.org/10.1038/s43017-020-0053-y

Claustre, H., Johnson, K. S., & Takeshita, Y. (2020). Observing the global ocean with biogeochemical-Argo. *Annual Review of Marine Science*, *12*(1), 23–48. https://doi.org/10.1146/annurev-marine-010419-010956

Cullen, J. (2001). Primary production methods. In J. H. Steele (Ed.), *Encyclopedia of ocean sciences* (pp. 2277–2284). Academic Press. https://doi.org/10.1006/rwos.2001.0203

de Boyer Montégut, C., Madec, G., Fischer, A. S., Lazar, A., & Iudicone, D. (2004). Mixed layer depth over the global ocean: An examination of profile data and a profile-based climatology. *Journal of Geophysical Research*, *109*(C12), C12003. https://doi.org/10.1029/2004JC002378

Estapa, M. L., Feen, M. L., & Breves, E. (2019). Direct observations of biological carbon export from profiling floats in the subtropical North Atlantic. *Global Biogeochemical Cycles*, *33*(3), 282–300. https://doi.org/10.1029/2018GB006098

Field, C. B., Behrenfeld, M. J., Randerson, J. T., & Falkowski, P. (1998). Primary production of the biosphere: Integrating terrestrial and oceanic components. *Science*, *281*(5374), 237–240. https://doi.org/10.1126/science.281.5374.237

Garcia, H., Locarnini, R., Boyer, T., Antonov, J., Baranova, O., Zweng, M., et al. (2014). Dissolved inorganic nutrients (phosphate, nitrate, silicate), *World ocean atlas* (Vol. 4, pp. 1–25). NOAA Atlas NESDIS.

Geider, R. J., & La Roche, J. (1994). The role of iron in phytoplankton photosynthesis, and the potential for iron-limitation of primary productivity in the sea. *Photosynthesis Research*, *39*(3), 275–301. https://doi.org/10.1007/bf00014588

Graff, J. R., Westberry, T. K., Milligan, A. J., Brown, M. B., Dall'Olmo, G., van Dongen-Vogels, V., et al. (2015). Analytical phytoplankton carbon measurements spanning diverse ecosystems. *Deep Sea Research Part I: Oceanographic Research Papers*, *102*, 16–25. https://doi.org/10.1016/j.dsr.2015.04.006

Groom, S., Sathyendranath, S., Ban, Y., Bernard, S., Brewin, R., Brotas, V., et al. (2019). Satellite ocean colour: Current status and future perspective. *Frontiers in Marine Science*, *6*, 485. https://doi.org/10.3389/fmars.2019.00485

Haëntjens, N., Boss, E., & Talley, L. D. (2017). Revisiting ocean color algorithms for chlorophyll *a* and particulate organic carbon in the Southern Ocean using biogeochemical floats. *Journal of Geophysical Research: Oceans*, *122*(8), 6583–6593. https://doi.org/10.1002/2017JC012844

Hostetler, C. A., Behrenfeld, M. J., Hu, Y., Hair, J. W., & Schulien, J. A. (2018). Spaceborne Lidar in the study of marine systems. *Annual Review of Marine Science*, *10*(1), 121–147. https://doi.org/10.1146/annurev-marine-121916-063335

IOCCG. (2008). Why ocean colour? In T. Platt, N. Hoepffner, V. Stuart, & C. Brown (Eds.), *The societal benefits of ocean-colour technology* (Vol. 7). https://doi.org/10.25607/OBP-97

Johnson, K. S., Plant, J. N., Coletti, L. J., Jannasch, H. W., Sakamoto, C. M., Riser, S. C., et al. (2017). Biogeochemical sensor performance in the SOCCOM profiling float array. *Journal of Geophysical Research: Oceans*, *122*(8), 6416–6436. https://doi.org/10.1002/2017jc012838

Johnson, K. S., Riser, S. C., Boss, E. S., Talley, L. D., Sarmiento, J. L., Swift, D. D., et al. (2020). SOCCOM float data—Snapshot 2020-04-20. In *Southern Ocean carbon and climate observations and modeling (SOCCOM) float data archive*. UC San Diego Library Digital Collections. https://doi.org/10.6075/J01G0JKT

Karl, D. M., Letelier, R. M., Bidigare, R. R., Björkman, K. M., Church, M. J., Dore, J. E., & White, A. E. (2021). Seasonal-to-decadal scale variability in primary production and particulate matter export at station aloha. *Progress in Oceanography*, *195*, 102563. https://doi.org/10.1016/j.pocean.2021.102563

Letelier, R. M., Karl, D. M., Abbott, M. R., & Bidigare, R. R. (2004). Light driven seasonal patterns of chlorophyll and nitrate in the lower euphotic zone of the North Pacific Subtropical Gyre. *Limnology & Oceanography*, *49*(2), 508–519. https://doi.org/10.4319/lo.2004.49.2.0508

Long, J. S., Fassbender, A. J., & Estapa, M. L. (2021). Depth-resolved net primary production in the northeast Pacific Ocean: A comparison of satellite and profiling float estimates in the context of two marine heatwaves. *Geophysical Research Letters*, *48*(19), e2021GL093462. https://doi.org/10.1029/2021GL093462

Marra, J. F., Barber, R. T., Barber, E., Bidigare, R. R., Chamberlin, W. S., Goericke, R., et al. (2021). A database of ocean primary productivity from the 14c method. *Limnology and Oceanography Letters*. https://doi.org/10.1002/lol2.10175

Martin, J., Gordon, R. M., & Fitzwater, S. E. (1990). Iron in Antarctic waters. *Nature*, *345*(6271), 156–158. https://doi.org/10.1038/345156a0

McClain, C. R. (2009). A decade of satellite ocean color observations. *Annual Review of Marine Science*, *1*(1), 19–42. https://doi.org/10.1146/annurev.marine.010908.163650

Moore, C. M., Mills, M. M., Arrigo, K. R., Berman-Frank, I., Bopp, L., Boyd, P. W., et al. (2013). Processes and patterns of oceanic nutrient limitation. *Nature Geoscience*, *6*(9), 701–710. https://doi.org/10.1038/ngeo1765

Morel, A., & Maritorena, S. (2001). Bio-optical properties of oceanic waters: A reappraisal. *Journal of Geophysical Research*, *106*(C4), 7163–7180. https://doi.org/10.1029/2000JC000319

Moseley, J. L., Allinger, T., Herzog, S., Hoerth, P., Wehinger, E., Merchant, S., & Hippler, M. (2002). Adaptation to Fe-deficiency requires remodeling of the photosynthetic apparatus. *EMBO Journal*, *21*(24), 6709–6720. https://doi.org/10.1093/emboj/cdf666

Ricchiazzi, P., Yang, S., Gautier, C., & Sowle, D. (1998). SBDART: A research and teaching software tool for plane-parallel radiative transfer in the Earth's atmosphere. *Bulletin of the American Meteorological Society*, *79*(10), 2101–2114. https://journals.ametsoc.org/view/journals/bams/79/10/1520-0477_1998_079_2101_sarats_2_0_co_2.xml

Riser, S. C., Swift, D., & Drucker, R. (2018). Profiling floats in SOCCOM: Technical capabilities for studying the Southern Ocean. *Journal of Geophysical Research: Oceans*, *123*(6), 4055–4073. https://doi.org/10.1002/2017JC013419

Roesler, C., Uitz, J., Claustre, H., Boss, E., Xing, X., Organelli, E., et al. (2017). Recommendations for obtaining unbiased chlorophyll estimates from in situ chlorophyll fluorometers: A global analysis of wet labs eco sensors. *Limnology and Oceanography: Methods*, *15*(6), 572–585. https://doi.org/10.1002/lom3.10185

Schrader, P. S., Milligan, A. J., & Behrenfeld, M. (2011). Surplus photosynthetic antennae complexes underlie diagnostics of iron limitation in a cyanobacterium. *PLoS One*, *6*(4), e18753. https://doi.org/10.1371/journal.pone.0018753

Steemann Nielsen, E. (1952). The use of radio-active carbon (C14) for measuring organic production in the sea. *ICES Journal of Marine Science*, *18*(2), 117–140. https://doi.org/10.1093/icesjms/18.2.117

Strzepek, R. F., Hunter, K. A., Frew, R. D., Harrison, P. J., & Boyd, P. W. (2012). Iron—Light interactions differ in Southern Ocean phytoplankton. *Limnology & Oceanography*, *57*(4), 1182–1200. https://doi.org/10.4319/lo.2012.57.4.1182

Tagliabue, A., Mtshali, T., Aumont, O., Bowie, A. R., Klunder, M. B., Roychoudhury, A. N., & Swart, S. (2012). A global compilation of dissolved iron measurements: Focus on distributions and processes in the Southern Ocean. *Biogeosciences*, *9*(6), 2333–2349. https://doi.org/10.5194/bg-9-2333-2012

Tagliabue, A., Sallée, J.-B., Bowie, A. R., Lévy, M., Swart, S., & Boyd, P. W. (2014). Surface-water iron supplies in the Southern Ocean sustained by deep winter mixing. *Nature Geoscience*, *7*(4), 314–320. https://doi.org/10.1038/ngeo2101

Veldhuis, M., Kraay, G., & Timmermans, K. (2001). Cell death in phytoplankton: Correlation between changes in membrane permeability, photosynthetic activity, pigmentation and growth. *European Journal of Phycology*, *36*(2), 167–177. https://doi.org/10.1080/09670260110001735318

Westberry, T., Behrenfeld, M. J., Siegel, D. A., & Boss, E. (2008). Carbon-based primary productivity modeling with vertically resolved photoacclimation. *Global Biogeochemical Cycles*, *22*(2), GB2024. https://doi.org/10.1029/2007GB003078

Xing, X., Claustre, H., Blain, S., D'Ortenzio, F., Antoine, D., Ras, J., & Guinet, C. (2012). Quenching correction for in vivo chlorophyll fluorescence acquired by autonomous platforms: A case study with instrumented elephant seals in the Kerguelen region (Southern Ocean). *Limnology and Oceanography: Methods*, *10*(7), 483–495. https://doi.org/10.4319/lom.2012.10.483

Yang, B., Fox, J., Behrenfeld, M. J., Boss, E. S., Haëntjens, N., Halsey, K. H., et al. (2021). In situ estimates of net primary production in the Western North Atlantic with Argo profiling floats. *Journal of Geophysical Research: Biogeosciences*, *126*(2), e2020JG006116. https://doi.org/10.1029/2020JG006116